1-1-2005

Electrochemical removal of zinc and nickel ions from wastewater using porous electrodes

Qazi Sabir
Ryerson University

ELECTROCHEMICAL REMOVAL OF ZINC AND NICKEL IONS FROM WASTEWATER USING POROUS ELECTRODES

by

Qazi Sabir, B.Eng.

Punjab University, Pakistan, 1995

A project report
presented to Ryerson University
in partial fulfillment of the
requirements for the degree of
Master of Engineering
in the Program of
Chemical Engineering

Toronto, Ontario, Canada, 2005

Author's Declaration

I hereby declare that I am the sole author of this project report.

I authorize Ryerson University to lend this report to other institutions or individuals for the purpose of scholarly research.

Qazi Sabir

I further authorize Ryerson University to reproduce this report by photocopying or by other means, in total or parts, at the request of other institutions or individuals for the scholarly research.

Qazi Sabir

Abstract

Simulated wastewater containing Ni^{++} and Zn^{++} was treated using an electrochemical cell. Porous aluminum cathode and porous stainless steel anode were used in a flow-through configuration. For porous cathodes, both aluminum foam and corrugated aluminum plates having perforations were used. To study the effects of applied voltage and volumetric liquid flux on the removal of Ni^{++} and Zn^{++}, the electrochemical cell was operated for 48 hours at different applied voltages of 5, 10, 12, 15, 20 and 25 V, and at different volumetric liquid fluxes both in the laminar (0.00471 and 0.00943 $m^3.m^{-2}.s^{-1}$) and turbulent regimes (0.01414, 0.01886 and 0.02357 $m^3.m^{-2}.s^{-1}$). For the maximum removal of both nickel and zinc ions, the optimum applied voltage and volumetric liquid flux were found to be 12 V and 0.02357 $m^3.m^{-2}.s^{-1}$, respectively; under these operating conditions, the concentrations of Ni^{++} and Zn^{++} in the simulated wastewater were reduced by 85.5 % and 98 % , respectively. Operating beyond an applied voltage of 12 V, the removal of Zn^{++} was slightly improved and achieved a maximum value of 99.05 % at 25 V; however, an opposite trend was observed in case of Ni^{++} removal, which finally decreased to 56% at 25 V., because of the excessive precipitation of Ni^{++} as nickel hydroxide.

Acknowledgements

The author would like to express his sincerest gratitude to Dr. Huu D. Doan for his invaluable scholarly assistance with regard to addressing several practical and theoretical problems that arose during the course of this project. Thanks are also due to the faculty and staff members of Department of Chemical Engineering, whose encouragement and moral support was a source of inspiration for the author.

Table of Contents

Author's Declaration....ii
Abstract....iii
Acknowledgements....iv
Table of Contents....v
List of Tables....vii
List of Figures....viii
Nomenclature....xi
1. Introduction....1
1.1. Industrial Effluent Discharge Limits....1
1.2. Conventional Treatment Technologies....2
1.3. Electrochemical Treatment....3
1.4. Objectives....4
2. Literature Review....5
2.1. Electrochemical Cell....5
2.2. Significance of Electrode Potential, Current Density and Cell Potential....5
2.3. Mass Transfer Aspects of Dilute Electrolytic Systems....9
2.4. Electrodes and Cell Designs for Heavy Metals Removal....13
2.5. Porous Electrodes for the Removal of Heavy Metals....16
3. Experimental....18
3.1. Experimental Apparatus....18
3.1.1. Electrochemical Cell....21
3.2. Experimental Procedure....22
3.2.1. Cleaning Prior to Experimental Runs....22
3.2.2. Preparation of Simulated Wastewater....23
3.2.3. Electrochemical Treatment....23
3.2.3.1. Temperature, Current and pH Measurements....24
3.2.3.2. Analysis of Zn^{++} and Ni^{++}....25
3.3. Viscosity and Density Calculations....26
3.4. Data Analysis....26

4. Results and Discussion.....27
4.1. Effect of Applied Voltage.....27
4.1.1. Effect of Applied Voltage on Removal of Zn^{++} and Ni^{++}.....27
4.1.2. Effect of Applied Voltage on Apparent Rate Constants 30
4.1.3. Applied Voltage and Anomalous Co-deposition.....33
4.1.4. Applied Voltage and Precipitation of Metal Ions.....35
4.2. Effect of Volumetric Liquid Flux.....38
4.2.1. Effect of Volumetric Liquid Flux on removal of Zn^{++} and Ni^{++}.....38
4.2.2. Effect of Volumetric Liquid Flux on Apparent Rate Constant (k) and Mass Transfer Coefficient (k_m).....44
4.3. Observed Deposits on the Cathode.....47
4.4. Comparison of Porous Corrugated Aluminum Cathode with Porous Aluminum Foam Cathode.....48
4.5. Optimum Voltage and Volumetric Liquid Flux.....50
5. Conclusions 55
6. Recommendations.....56
References.....57
Appendices.....63
Appendix A: Sample Calculations.....63
Appendix A1: Orifice Diameter Calculation.....63
Appendix A2: Calculation of Surface Area of the Anode.....64
Appendix A3: Viscosity and Density Calculations 64
Appendix A4: Calculation of Volumetric Liquid Flux and Reynolds Number.....66
Appendix A5: Rate of Reaction Calculation.....67
Appendix A6: Calculation of the Mass Transfer Coefficient 68
Appendix A7: Uncertainty in Mass Transfer Coefficient.....69
Appendix B: Summary of Experimental Runs 72
Appendix B1: Porous Aluminum Foam Cathode and Porous SS Anode.....72
Appendix B2: Porous Corrugated Aluminum Cathode and Porous SS Anode.....73

List of Tables

Table 1.1 Industrial effluent discharge limits for nickel and zinc Ions.....2

Table 4.1: Apparent rate constants for Zn^{++} and Ni^{++}.....30

Table 4.2: Effect of applied voltage on metal ions precipitation after 48 hours of electrochemical treatment.....37

Table 4.3: Apparent rate constants (k) and mass transfer coefficients (k_m) for Zn^{++} and Ni^{++}.....44

Table 4.4: Comparison between apparent rate constants and mass transfer coefficients for Zn^{++} and Ni^{++} at 10 and 12 V, and at a constant volumetric flux of 0.02357 $m^3.m^{-2}.s^{-1}$.....50

Table A4-1: Volumetric liquid fluxes and Reynolds numbers at different flow rates (D_{Cell} =.0.15m; A_{Cell} = 0.01767 m^2; $\upsilon = 8.72\times10^{-7}\ m^2.s^{-1}$).....67

Table A6-1: Mass transfer coefficient for Zn^{++}.....68

Table B1-1: Run 1.....72

Table B1-2: Run 2.....72

Table B1-3: Run 3.....73

Table B2-1: Run 1.....73

Table B2-2: Run 2.....74

Table B2-3: Run 3.....74

Table B2-4: Run 4.....75

Table B2-5: Run 5.....75

Table B2-6: Run 6.....76

Table B2-7: Run 7.....76

Table B2-8: Run 8.....77

Table B2-9: Run 9.....77

Table B2-10: Run 10.....78

List of Figures:

Fig 2.1: Idealized Polarization Curve.....9
Fig 2.2: (a) Tank Cell.....13
Fig 2.2: (b) Monopolar.....13
Fig 2.2: (c) Bipolar.....13
Fig 2.3: Plate and Frame Cell.....14
Fig 2.4: Rotating Cylinder Cell.....14
Fig 2.5: (Chemlec) Fluidized Bed Cell.....14
Fig 2.6: Packed Bed Cell.....15
Fig 2.7: Swiss Roll Electrode.....15
Figure 3.1: Schematic diagram of the experimental apparatus for electrochemical treatment of simulated wastewater (Dashed (--) lines represent the wires connecting anode and cathode to direct current power supply).....19
Figure 3.2: Different arrangements of the orifices at the bottom of the electrochemical cell with respect to different volumetric liquid fluxes (dark and light colored circles show closed and open orifices, respectively).....20
Fig 3.2(a): Arrangement for volumetric liquid fluxes of 0.00471 and 0.00943 $m^3.m^{-2}.s^{-1}$... 20
Fig 3.2(b): Arrangement for volumetric liquid flux of 0.01414 $m^3.m^{-2}.s^{-1}$.....20
Fig 3.2(c): Arrangement for volumetric liquid flux of 0.01886 $m^3.m^{-2}.s^{-1}$.....20
Fig 3.2(d): Arrangement for volumetric liquid flux of 0.02357 $m^3.m^{-2}.s^{-1}$.....20
Figure 3.3: Corrugated aluminum plate perforations.....22
Figure 4.1: Effect of applied voltage on Zn^{++} removal during electrochemical treatment using porous corrugated aluminum cathode and SS anode at volumetric liquid flux of 0.02357 $m^3.m^{-2}.s^{-1}$ (T = 25°C; pH = 5.6-6; I = 0.044, 0.155, 0.260, 0.360 and 0.470 A at applied voltages of 5, 10 ,15 ,20 and 25V, respectively).....28
Figure 4.2: Linear regression for Zn^{++}: Effect of applied voltage during electrochemical treatment using porous corrugated aluminum cathode and SS anode at volumetric liquid flux of 0.02357 $m^3.m^{-2}.s^{-1}$ (T = 25°C; pH = 5.6-6; I = 0.044, 0.155, 0.260, 0.360 and 0.470 A at applied voltages of 5, 10 ,15 ,20 and 25V, respectively). Solid line is linear regression 29

Figure 4.3: Effect of applied voltage on Ni^{++} removal during electrochemical treatment using porous corrugated aluminum cathode and SS anode at volumetric liquid flux of 0.02357 $m^3.m^{-2}.s^{-1}$ (T = 25°C; pH = 5.6-6; I = 0.044, 0.155, 0.260, 0.360 and 0.470 A at applied voltages of 5, 10 ,15 ,20 and 25V, respectively).....31

Figure 4.4: Linear regression for Ni^{++}: Effect of applied voltage during electrochemical treatment using porous corrugated aluminum cathode and SS anode @ volumetric liquid flux of 0.02357 $m^3.m^{-2}.s^{-1}$ (T = 25°C; pH = 5.6-6; I = 0.044, 0.155, 0.260, 0.360 and 0.470 A at applied voltages of 5, 10 ,15 ,20 and 25V, respectively). Solid line is linear regression.....32

Figure 4.5: Effect of volumetric liquid flux on Zn^{++} removal during electrochemical treatment using porous corrugated aluminum cathode and SS anode at an applied voltage of 10 V (T = 25°C; pH = 5.6-6; I = 0.155 A).....39

Figure 4.6: Linear regression for Zn^{++}: Effect of volumetric liquid flux during electrochemical treatment using porous corrugated aluminum cathode and SS anode at an applied voltage of 10 V (T = 25°C; pH = 5.6-6; I = 0.155 A). Solid line is linear regression.....40

Figure 4.7: Effect of volumetric liquid flux on Ni^{++} removal during electrochemical treatment using porous corrugated aluminum cathode and SS anode at an applied voltage of 10 V (T = 25°C; pH = 5.6-6; I = 0.155 A) 41

Figure 4.8: Linear regression for Ni^{++}: Effect of volumetric liquid flux during electrochemical treatment using porous corrugated aluminum cathode and SS anode at an applied voltage of 10 V (T = 25°C; pH = 5.6-6; I = 0.155 A). Solid line is linear regression.....42

Figure 4.9: Comparison between Zn^{++} and Ni^{++} removal in the laminar and turbulent flow regimes during electrochemical treatment using porous corrugated aluminum cathode and SS anode at an applied voltage of 10 V (T = 25°C; pH = 5.6-6; I = 0.155 A).....43

Figure 4.10: Effect of volumetric liquid flux on mass transfer coefficients for Zn^{++} and Ni^{++} during electrochemical treatment using porous corrugated aluminum cathode and SS anode at an applied voltage of 10 V (T = 25°C; pH = 5.6-6; I = 0.155A).....45

Figure 4.11: Comparison between Porous Corrugated Aluminum Cathode and Porous Aluminum Foam Cathode: at different volumetric liquid fluxes and an applied voltage of 10 V (T = 25°C; pH = 5.6-6).....49

Figure 4.12: Effect of applied voltage on removal of Zn^{++} and Ni^{++} after 48 hours of electrochemical treatment using porous corrugated aluminum cathode and SS anode at volumetric liquid flux of 0.02357 $m^3.m^{-2}.s^{-1}$ (T = 25°C; pH = 5.6-6; I = 0.044, 0.155, 0.260, 0.360 and 0.470 A at applied voltages of 5, 10 ,15 ,20 and 25V, respectively).....51

Figure 4.13: Comparison of Zn^{++} and Ni^{++} removal at 10 and 12 V during electrochemical treatment using porous corrugated aluminum cathode and SS anode at volumetric liquid flux of 0.02357 $m^3.m^{-2}.s^{-1}$ (T = 25°C; pH = 5.6-6; I = 0.155 and 0.195 A at applied voltages of 10 and 12 V, respectively).....52

Figure 4.14: Linear regression for Zn^{++} and Ni^{++}: Effect of an applied voltage of 12 V during electrochemical treatment using porous corrugated aluminum cathode and SS anode at volumetric liquid flux of 0.02357 $m^3.m^{-2}.s^{-1}$ (T = 25°C; pH = 5.6-6; I = 0.195 A). Solid line is linear regression.....53

Nomenclature

Symbol	Description
A	Electrode area (m^2)
A_C	Electrode area per unit volume of the reactor (m^2/m^3)
A_{Cell}	Area of the electrochemical cell (m^2)
c	Concentration ($mg.l^{-1}$)
C_b	Concentration in the bulk liquid phase ($mg.l^{-1}$)
C_0	Initial concentration at time t = 0 ($mg.l^{-1}$)
C_O	Concentration of the reduced species ($mg.l^{-1}$)
C_R	Concentration of the oxidized species ($mg.l^{-1}$)
C_S	Concentration at the electrode surface ($mg.l^{-1}$)
C_t	Concentration at time t ($mg.l^{-1}$)
D	Diffusion coefficient ($m^2.s^{-1}$)
D_C	Characteristic diameter (m)
D_{cell}	Diameter of the electrochemical cell (m)
e^-	Electron
E'	Electrode potential (V)
E^e	Equilibrium potential (V)
E^e_A	Equilibrium electrode potential of anode (V)
E^e_C	Equilibrium electrode potential of cathode (V)
E^e_{cell}	Equilibrium cell potential (V)
E^0	Standard reduction potential (V)
E_m	Metal potential (V)
E_S	Solution potential (V)
F	Faraday's constant (96,485 $A.s.mol^{-1}$)
G	Gibb's free energy ($J.mol^{-1}$)
i	Current density ($A.m^{-2}$)

i_{lim}	Limiting current density ($A.m^{-2}$)
I	Current (A)
k	Reaction rate or apparent rate constant (s^{-1})
k_m	Mass transfer coefficient ($m.s^{-1}$)
m	Amount of metal (mg)
M	Molecular weight
n	Number of electrons
N	Molar flux ($mol.s^{-1}.m^{-2}$)
O	Species that becomes reduced
P	Pressure ($lb.ft^{-2}$)
Q	Liquid flow rate ($m^3.s^{-1}$)
r	Rate of reaction ($kg.m^{-2}.s^{-1}$)
R	Species that becomes oxidized
R	Gas constant ($8.314\ J.K^{-1}.mol^{-1}$)
Re	Reynolds number
T	Temperature (K)
t	Time (s)
ψ	Mobility ($m^2.s^{-1}.V^{-1}$)
u	Characteristic velocity ($m.s^{-1}$)
U	Volumetric liquid flux ($m3.m^{-2}.s^{-1}$)
v	Bulk fluid velocity ($m.s^{-1}$)
V	Volume (m^3)
Y_{ST}	Space-time yield ($kg.m^{-3}.s^{-1}$)
z	Charge on the ion (Coulomb)

Greek Symbols

η	Overpotential (V)
η_{act}	Activation overpotential (V)
η_{conc}	Concentration overpotential (V)
η_{ohm}	Ohmic overpotential (V)

$\nabla\phi$	Potential gradient (V)
δ	Nernst diffusion layer thickness (Angstrom)
ρ	Liquid density ($kg.m^{-3}$)
υ	Kinematic viscosity ($m^2.s^{-1}$)
ξ_C	Current efficiency

Subscripts

a	Anode
act	Activation
conc	Concentration
b	Bulk
c	Cathode; current
cell	Cell
i	Species
lim	Limiting
m	Metal; mass transfer
O	Reduced species
ohm	Ohmic
R	Oxidized species
S	Surface; solution
ST	Space-time

Superscripts

e	Equilibrium
0	Standard

Abbreviations

ppi	Pores per inch
ppm	Parts per million
SS	Stainless steel

1. Introduction

Effluents from industrial processes and hydrometallurgical operations, such as metal finishing, electroplating and mining, contain heavy metals. Most of the heavy metals, for instance, mercury, lead, cadmium, or nickel, are toxic in nature and pose long-term environmental and health hazards. The removal of heavy metals from the aforementioned effluents is important, not only from environmental viewpoint, but also for economic reasons as the recovery of these metals can minimize operational costs [1].

The present study deals with the electrochemical treatment of wastewater generated from an electro-coating process used in the automotive industry. Electro-coating provides corrosion resistance to automobiles' parts and bodies. The electro-coating process involves cleaning, coating and rinsing of the metal parts; copious amounts of wastewater are generated during these steps, especially during rinsing [2]. In the electro-coating process, zinc-nickel alloys are the most commonly used protective coatings [3]. Therefore, the wastewater from the coating process typically contains nickel and zinc ions.

Depending on the plant capacity, the flow rate of a wastewater stream leaving an automotive plant can be very large. For instance, at the Toyota plant in Georgetown, Kentucky, 1.4 million gallons of wastewater is generated per day [4]. Automotive-parts industry is one of the major manufacturing sectors in southern Ontario; in this industry, the electro-coating process generates 0.25 gallons of wastewater per square foot of the metal parts being coated [5].

1.1. Industrial Effluent Discharge Limits

The effluent discharge limits are becoming ever more stringent due to rapid increase in the quantities of industrial wastewater. The concentration of metal ions has to be reduced to a permissible maximum before discharging the wastewater to a sewer. In 2003, United States Environmental Protection Agency (US EPA) imposed stringent daily effluent discharge limits for existing Metal Products and Machinery (MP&M) sector. Table 1.1 summarizes the current (2003) [6] and previous (before 2003) [2] maximum daily

discharge limits for zinc and nickel in the MP&M sector. Discharge limits for zinc and nickel in the sanitary sewer were enacted by the Council of the City of Toronto in 2000 [7]; for comparison, these limits (current: 2000; previous: before 2000) are also provided in Table 1.1.

Table 1.1 Industrial effluent discharge limits for nickel and zinc ions

Jurisdiction	Ionic species	Daily maximum: current ($mg.l^{-1}$)	Daily maximum: previous ($mg.l^{-1}$)
City of Toronto Limits [7]	Zinc	2	4
	Nickel	2	4
US EPA MP&P Limits [2 and 6]	Zinc	0.35	4.2
	Nickel	1.5	4.1

1.2. Conventional Treatment Technologies

Metal ion solutions from an electro-coating process are commonly treated by chemical and physical processes, such as chemical precipitation, ultrafiltration, solvent extraction, reverse osmosis and ion exchange. Among the aforementioned processes, chemical precipitation is most widely used because of its simplicity and cheapness; this method involves precipitation of dissolved metal ions as hydroxides, sulfides or carbonates, followed by separation and dehydration of the formed sludge [4, 8, 9].

Nevertheless, chemical precipitation process has few drawbacks. As precipitation of most metals occurs in a pH range of 8.5 to 10, continuous adjustment of the wastewater pH is required. Further chemical treatment is required to readjust the pH of the wastewater between 6.0 and 7.0 before discharging it to the sewer. The whole process requires extensive use of chemicals for pH adjustment. These ultimately become part of the sludge that has no real use, and its disposal involves other environmental problems. Moreover, the process is unable to meet the effluent discharge limits if the wastewater to be treated contains a mixture of dissolved metals, for each dissolved metal precipitates at a corresponding optimum pH, whereas hydroxide precipitation is usually carried out at a

compromised pH [2, 5, 10]. This situation necessitates the development of new and efficient techniques for the treatment of wastewater.

1.3. Electrochemical Treatment

Over the past few years, electrochemical technology has emerged as an efficient technique for the treatment of wastewater. Common electrochemical technologies for the treatment of wastewater containing dissolved metal ions are electrodeposition, electrocoagulation, electroflotation and electrowinning [11, 12].

Electrodeposition involves the recovery of heavy metals from wastewater through cathodic deposition. Electrocoagulation utilizes direct current for in situ generation of sacrificial ions from electrodes. The sacrificial ions act as coagulants to remove dissolved metal ions. In electroflotation process, tiny bubbles of hydrogen and oxygen gases are generated by water electrolysis. The generated bubbles make the pollutants to float to the surface of the wastewater. Electrowinning is based on the method of electrodeposition, and is mainly used in mining industry to extract dissolved metals from ore leaching liquid. This method has also been employed to remove metal ions from industrial effluents [12-14].

The most attractive features of the electrochemical processes are [9, 10]:

- Versatility
- High efficiency
- Amenability to automation
- Clean operation as opposed to sludge formation in chemical precipitation
- Possibility of recovering pure metal from effluents

Further research in the field of metal recovery from wastewater revolves around designing better electrochemical reactors with enhanced space-time yield, which, in turn, necessitates the development of electrodes having large surface area and improved mass transfer characteristics.

1.4. Objectives

As already stated, the wastewater generated from an electro-coating process typically contains nickel and zinc ions; the reduction of heavy metals from this wastewater can be accomplished through electrodeposition. The electrochemical treatment of electro-coating wastewater was previously investigated by Doan *et al.* [5], who used flat plate electrodes for reduction of nickel and zinc. In continuation of their work, Mitzakov [15] employed porous electrodes with "plate-in-tank" configuration and investigated the effect of volumetric liquid flux on the removal of nickel and zinc. However, he did not find porous electrodes, with "plate-in-tank" configuration, to be a viable option for concurrent removal of nickel and zinc.

The present study, which is a continuation of Mitzakov's work [15], employs porous electrodes in a "flow-through" configuration. The treatment of dilute aqueous metal solutions is a mass-transfer limited phenomenon. Improving mass transport in dilute solutions would require either increased turbulence or increased electrode surface area. Therefore, in the present work porous electrodes are used in "flow-through" configuration to achieve improved mass transfer kinetics. The main objectives of the present study are:

- To investigate the effect of applied voltage on removal of nickel and zinc ions.
- To study the effect of volumetric liquid flux on removal of nickel and zinc ions.
- To investigate the effects of applied voltage and volumetric liquid flux on rate constants for nickel and zinc removal, and to compare the values of mass transfer coefficients for nickel and zinc obtained in the present study with those reported in the literature for Ni-Zn system.
- To find the optimum applied voltage and volumetric liquid flux for concurrent reduction of nickel and zinc ions.

2. Literature Review

2.1. Electrochemical Cell

An electrochemical cell consists of at least two electrodes, an electrolyte, and external wiring and loads. The electrode at which the current enters the cell is the anode, and the one at which it leaves is the cathode. The liquid phase that completes the circuit between electrodes is called the electrolyte.

Electrode reactions, or oxidation-reduction reactions, are heterogeneous in nature and occur in the interfacial region between electrode and solution, the region where charge distribution differs from that of the bulk phase [16]. In oxidation-reduction reactions, there is loss and gain of electrons between two species; a decrease occurs in the oxidation number of the species that gains electrons, while an increase occurs in the oxidation number of the species that loses electrons. A typical oxidation-reduction reaction between two species, O and R, is shown in equation 2.1

$$O + ne^- \longleftrightarrow R \tag{2.1}$$

where n corresponds to number of electrons (e^-)

The reduction of species occurs at the cathode. It is also called cathodic reduction. Similarly, oxidation of species occurs at the anode. It is also called anodic oxidation. These coupled reactions produce an electric current, which is the flow of electrons through a circuit.

2.2. Significance of Electrode Potential, Current Density and Cell Potential

Consider the interfacial region between electrode and electrolyte. The electrode potential (E') is referred to as the difference between the metal potential (E_m) and the solution potential (E_S) [17]:

$$E' = E_m - E_S \tag{2.2}$$

At the cathode, positive current flows from the electrolyte to the electrode. Therefore, by definition of equation 2.2, electrode potential for a cathode tends to be negative, whereas it is positive for an anode.

Another important conclusion that can be drawn from equation 2.2 is that if the electrode potential is kept constant and the area of electrode is doubled, the current flowing between the electrode and electrolyte is also doubled. In other words, with other parameters remaining constant, the current supported by an electrode is proportional to its area. This is why the current carried by unit area of electrode is a more fundamental property than the total current; it is referred to as current density (i), which is a measure of the rate of an electrochemical process.

The spontaneity or non-spontaneity of oxidation-reduction reactions depend on cell potential and are related to Gibbs free energy change of the system. The equilibrium cell potential (E^e_{cell}) is referred to as the difference between the equilibrium electrode potentials of cathode (E^e_C) and anode (E^e_A). The following expression provides the relation between Gibbs free energy change (ΔG) and equilibrium cell potential [18]:

$$\Delta G = -nFE^e_{cell} = -nF(E^e_C - E^e_A) \tag{2.3}$$

For a process to be spontaneous, the change in Gibbs free energy must be less than zero. This requires a positive value for the equilibrium cell potential. If the equilibrium cell potential is negative, the change in Gibbs free energy of the system will be positive, indicating a non-spontaneous process. In such situation, an external power source is required to provide a potential greater than the potential that a spontaneous reverse reaction would produce.

Since there is no means of measuring an absolute electrode potential, the standard reduction potentials (E^0) are measured relative to a hydrogen electrode. An arbitrary

value of zero volts is assigned to the hydrogen electrode. Equations 2.4 and 2.5 show the standard reduction potentials for zinc and nickel at 25°C [19]:

$$Zn^{2+} + 2e^{-} \longrightarrow Zn \qquad E^{0} = -0.76\,V \tag{2.4}$$

$$Ni^{2+} + 2e^{-} \longrightarrow Ni \qquad E^{0} = -0.23\,V \tag{2.5}$$

Both nickel and zinc have negative reduction potentials; based on the above equations, zinc would have a greater tendency to lose electrons than nickel. In other words, zinc has greater reducing strength than nickel.

In most of the situations involving oxidation-reduction reactions, the reduction potentials of the oxidized and reduced species are not in their standard states; to account for these situations, the following Nernst equation is used [18]:

$$\Delta E^{e} = \Delta E^{0} - \frac{RT}{nF}\ln\left(\frac{C_R}{C_O}\right) \tag{2.6}$$

When an electric current flows through an electrode, it causes a change in its equilibrium potential (E^{e}). This shift is referred to as an overvoltage or overpotential (η) that depends on the ohmic resistance of the electrolyte (η_{ohm}), the activation energy barrier limitations (η_{act}), and the concentration effects through mass transport limitations (η_{conc}). The overvoltage is a sum of these factors [20]:

$$\eta = \eta_{ohm} + \eta_{act} + \eta_{conc} \tag{2.7}$$

It is related to the electrode potential by the following expression:

$$E' = E^{e} + \eta_{ohm} + \eta_{act} + \eta_{conc} \tag{2.8}$$

The terms η_{ohm}, η_{act} and η_{conc} always represent energy and voltage losses.

The first term η_{ohm} represents losses due to the resistance of the electrolyte; losses due to resistances of the electrode, wiring and external loads are also included in this term.

The second term η_{act} represents losses due to slow kinetics of electrochemical reactions, which, in turn, are linked to large energy activation barrier. To overcome slow kinetics, either the applied voltage across the electrodes is increased, or the temperature is increased. In both cases, additional energy is required to achieve better reaction kinetics.

The third term η_{conc} is associated with losses due to mass transfer limitations. When voltage is applied to an electrode, the charges, which accumulate on the surface of the electrode, attract ions of the opposite charges from the electrolyte. In due course, opposite charges and ions align themselves on the surface of the electrode and in the interfacial region respectively, and a double layer is formed. The reaction takes place across this double layer. For a fast electrode reaction, a reactant must be replaced at an appreciable rate in order to maintain the reaction. Therefore, for dilute solutions, the mass transport becomes a limiting factor. The solution lies in decreasing the thickness of that double layer. This is often accomplished by creating turbulence, or increasing electrolyte flow rate.

Information about the kinetics of electrode reactions can often be obtained by plotting current density (i) or ln (i) against overpotential (η). The curve thus obtained (see Figure. 2.1) is called a polarization curve [17].

The initial linear rise in current density in Figure 2.1 corresponds to conditions when the rate limiting step is the rate of charge transfer. The horizontal portion, where the current density becomes independent of the overpotential, represents a situation where mass transfer is rate controlling; at this point the limiting current (i_{lim}) is reached. Applying greater potential beyond this point would eventually lead to parasitic reactions, such as hydrogen evolution.

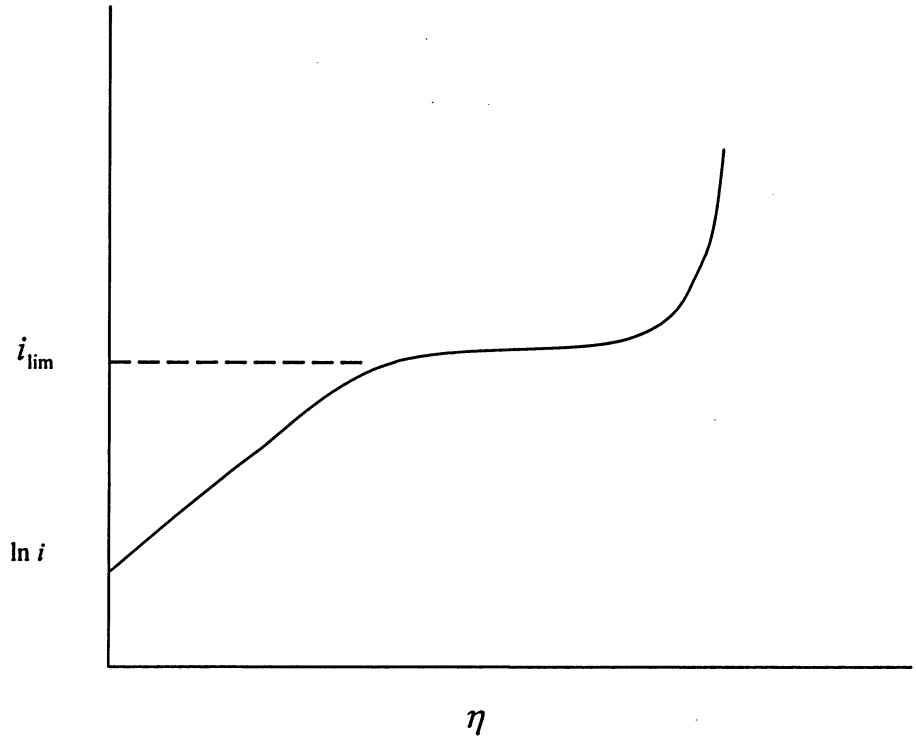

Figure 2.1 Idealized Polarization Curve, i = current density, i_{lim} = limiting current density, η = overpotential [17]

2.3. Mass Transfer Aspects of Dilute Electrolytic Systems

In an electrochemical reactor, the transfer of a species, from the bulk electrolyte to the electrode surface, can be affected by three mechanisms [16]:

- Molecular diffusion under the influence of concentration gradient
- Migration of charged species under the influence of a potential gradient
- Convection due to convective movement of the fluid

One common description of an electrochemical system is derived from assuming that the concentrations of electroactive species are extremely small. Under these conditions, an expression for describing the flux of a species is [19]:

$$N_i = -z_i \psi_i F c_i \nabla\phi - D_i \nabla c_i + c_i v \tag{2.9}$$

where N_i is the flux of species i, z_i is the charge on species i, ψ_i is the mobility of species i, c_i is the concentration of species i, D_i is the diffusivity of species i, F is the Faraday's constant, $\nabla\phi$ is the potential gradient, , and v is the bulk fluid velocity. Flux, potential gradient, and fluid velocity are vector quantities, indicated by bold face type. The terms on the right side of the equation represent fluxes resulting from migration, diffusion and convection, respectively. Equation 2.9 is also called flux density equation.

In case of infinitely dilute metal solutions, diffusion due to concentration gradient is negligible. Mass transport due to migration of charged species can be improved with the use of a supporting electrolyte; supporting electrolyte may be defined as an inert substance that does not take part in the electrode reactions, and helps increase the conductivity of the bulk electrolyte by minimizing ohmic resistances. The mass transfer can be improved by increasing convection, and as already stated, its importance lies in reducing the thickness of the double layer that forms adjacent to the surface electrode under laminar flow conditions.

A much simplified version of the flux density equation (Eq.2.9), which takes into account only convective transport of the species *i* from the bulk electrolyte to electrode surface, is given by

$$N_i = k_m (C_b^i - C_s^i) \tag{2.10}$$

where C_b^i and C_s^i are the concentrations of species i in the bulk and at the electrode surface, respectively, k_m is the mass transfer coefficient and is given by

$$k_m = \left(\frac{D}{\delta}\right) \tag{2.11}$$

where D is the diffusion coefficient and δ is the Nernst diffusion layer thickness

According to Faraday's law, the current density at an electrode is proportional to ion flux

$$i = nFN_i \tag{2.12}$$

Combining equations (2.10) and (2.12) gives the relation between mass transfer coefficient and current density

$$k_m = \frac{i}{nF(C_b^i - C_s^i)} \tag{2.13}$$

Under limiting current conditions (with $i = i_{\text{lim}}$), the concentration of the electroactive species at the electrode surface becomes zero ($C_s^i = 0$), and the process becomes mass transfer controlled

$$k_m = \frac{i_{\text{lim}}}{nFC_b^i} \tag{2.14}$$

However, in case of extremely dilute metal ion solutions, the rate of mass transport controlled processes greatly decreases. The challenge lies in increasing the performance of an electrolytic reactor by improving current efficiency and space-time yield [17].

Current efficiency (ξ_C) is defined as the ratio of theoretical amount of current required to produce a target product to that of actual consumption of the current during the electrolytic process. Current efficiency indicates both the specificity of a process and the performance of an electrolytic process involving surface reaction as well as mass transfer.

For the cathodic metal deposition in an electrochemical reactor, the space- time yield (Y_{ST}) is defined as the amount of metal deposited (dm) in time interval (dt) per unit volume (V) of the reactor [10]:

$$Y_{ST} = \frac{1}{V}\frac{dm}{dt} \tag{2.15}$$

According to Faraday's law, dm is proportional to the electrolysis charge $A\xi_c\, i\, dt$:

$$dm = A\xi_c\, i\, dt \frac{M_i}{nF} \tag{2.16}$$

where A is the actual electrode area, and M_i is the molecular weight of the metal deposited.

At the limiting current density, the optimal process conditions are met when the rate of heterogeneous process attains it maximum. Thus, replacing i *with* i_{lim} in equation (2.16) and combining it with equations (2.14) and (2.15), the final expression for space-time yield is given by:

$$Y_{ST} = \xi_c M_i A_c k_m C_b^i \tag{2.17}$$

Equation (2.17) provides a key relation for design of an electrochemical reactor for wastewater treatment and metal recovery. For a given metal ion concentration, a high mass transfer coefficient k_m, and a large specific electrode area A_C ($A_C = A/V$) are essential to achieve high space-time yields. In the recent years, major research activities in the field of heavy metal recovery from wastewater have revolved around designing electrodes and cells that exhibit improved mass transfer characteristics.

2.4. Electrodes and Cell Designs for Heavy Metals Removal

Different electrodes and cell designs have been reported in the literature [10, 11, 21]. Efforts in efficient cell design have been directed towards the optimization of the space-time yield according to the key formula provided in equation (2.17), i.e. high specific electrode area and/or large mass transfer coefficient.

It is not possible to review all types of cell designs; only a few are discussed here that have found application in metal recovery; these include basic electrochemical cells, such as tank cells, plate and frame cells, rotating cells, and more complicated three-dimensional systems, for instance, fluidized bed cells, packed bed cells, perforated cells, or porous carbon cells.

Tank cell (Figure 2.2a) represents the simplest and the most popular cell design. One great advantage of this system is that it can be easily scaled up or down depending upon the load of the process. The electrodes may be arranged in monopolar or bipolar mode (Figures. 2.2 (b) and 2.2 (c)), and their number may vary from 10 to 100 in a stack [11].

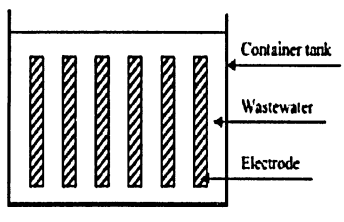

Fig 2.2 (a) Tank Cell [11]

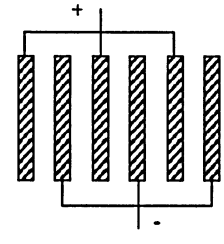

Fig 2.2 (b) Monopolar [11]

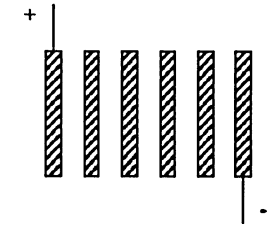

Fig 2.2 (c) Bipolar [11]

Plate and frame cell (Figure 2.3), also called filter press, is another other popular electrochemical cell design. The cell consists of a number of modules, with each module having an anode, a cathode, and a membrane. This module arrangement makes the design, operation and maintenance of the cell relatively simple.

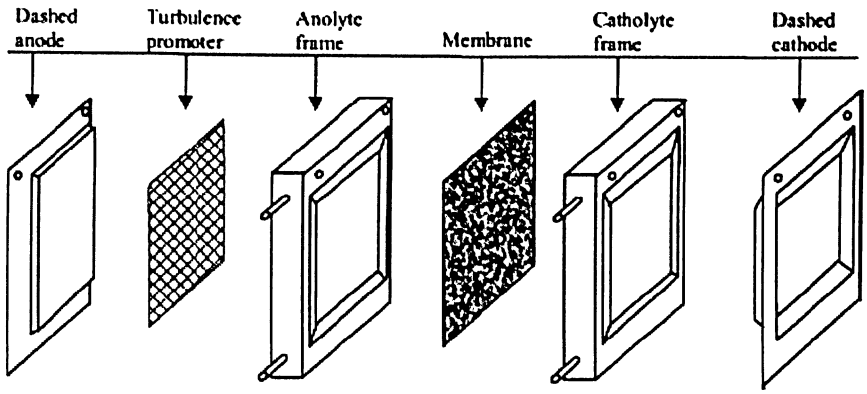

Fig 2.3 Plate and Frame Cell [11]

In rotating cylinder cell (Figure 2.4), the cathode for metal deposition rotates between the anodes. The rotation enhances turbulence, which results in increased mass transfer for the metal ions from the bulk to the electrode surface. The deposited metal then can be scraped off the electrode surface with the aid of a scraper blade [21].

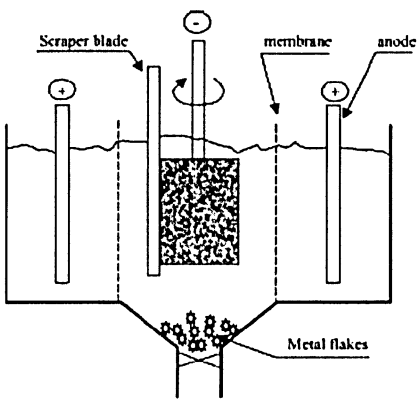

Fig 2.4 Rotating Cylinder Cell [11]

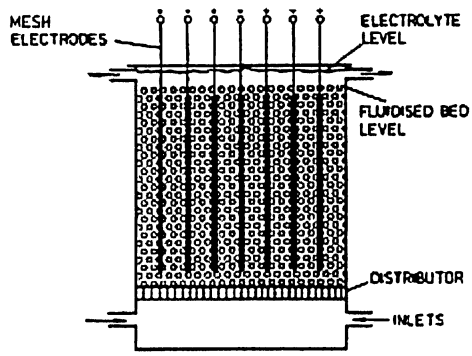

Fig 2.5 (Chemlec) Fluidized Bed Cell [10]

The Chemlec cell (Figure 2.5) uses a fluidized bed of glass spheres, which act as turbulence promoters to improve the mass transfer to the electrodes. The electrodes consist of a series of closely spaced gauze, or expanded metal sheet electrodes. Because of the fluidization of the particles by water flow, the electric contact can not be maintained at all times, which results in poor distribution of the current and large ohmic drop within the cell.

The packed bed cell (Figure 2.6) overcomes the non-contacting problem encountered in the fluidized bed cell. In packed bed cells, porous electrodes comprising electron conducting particulate material are used. Either flow-through or flow-by arrangement is used; in flow-through configuration, the current is parallel to the flow of electrolyte, whereas in flow-by configuration, the current is perpendicular to the flow of electrolyte. In case of packed bed cell, usually flow-by arrangement is preferred due to minimization of ohmic losses.

Swiss roll electrode design (Figure 2.7) represents an efficient way of fitting a large planar electrode area in a small volume. Thin metal foils, separated by an electrolyte-permeable plastic mesh, are wrapped around a central core. The electrodes are contacted at opposite ends to compensate for inhomogeneous potential distribution due to ohmic drop. The Swiss role electrode is placed vertically in a cylinder. The electrolyte flows axially through the electrode pack. The plastic separator mesh serves as turbulence promoter and helps increase mass transfer rates and space-time yield. The performance of the cell can be further increased by employing perforated electrodes, which give it a three-dimensional character. Thus, meshed electrodes wrapped around a perforated winding core form another version of the Swiss roll cell with radial flow.

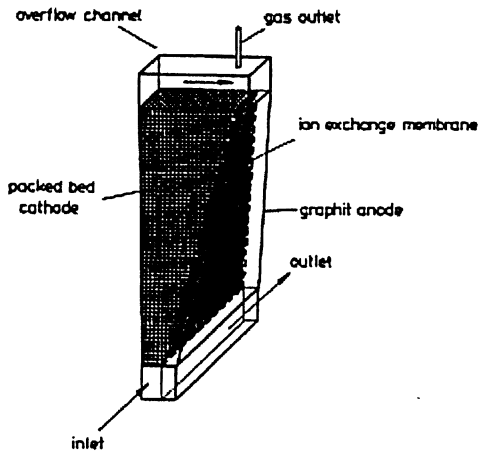

Fig 2.6 Packed Bed Cell [10]

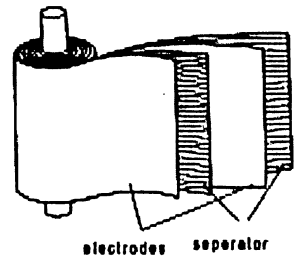

Fig 2.7 Swiss Roll Electrode [10]

In general, for the removal of heavy metals from dilute wastewater streams, extended surface area porous electrodes offer practical advantages over slab-like two-dimensional or planar electrodes. In contrast to planar electrodes, three-dimensional porous electrodes have large specific surface area and exhibit improved mass transfer characteristics.

2.5. Porous Electrodes for the Removal of Heavy Metals

There is a broad definition for the term "porous electrodes" frequently used in the literature. It may refer to a packed bed of particles, intermeshing elements as in steel wool, a regular array of perforated plate electrodes, or a continuous porous matrix of reticulated materials of metal or carbon [18]. A variety of materials have been used for porous electrodes; these include carbon and graphite felts [22-26], nickel felts [27], iron felts [28, 29], stacked nets or screens [30-32] or carbon cloth [33], packed beds of either nickel or graphite [34, 35], reticulated vitreous carbon [36-41] and metallic foams [42-46].

The use of porous electrodes for the removal of heavy metals from dilute aqueous streams was pioneered by Bennion and Newman [47]; in their study, they employed a porous flow-through fixed-bed of graphite chips for removal of copper ions from dilute solutions. Since then, the porous electrodes have been applied for the removal of a variety of metallic ions such as copper, mercury, lead, zinc, and nickel; a few examples are presented in the following paragraphs.

Panizza *et al.* [45] used polyurethane foam coated with a thin layer of copper as porous electrode; they used a batch recycle mode and were able to reduce the initial copper concentration by 98 %. Other researchers have also demonstrated the successful use of porous electrodes for removal of copper. Simonsson [35] utilized a particulate bed electrode, which was composed of graphite grains, to reduce copper from a copper sulfate solution from an initial copper concentration of 67 $mg.l^{-1}$ to a final concentration of 0.03 $mg.l^{-1}$. Al-Shammari *et al.* [48] investigated the effect of applied voltage on removal of copper from simulated wastewater using a perforated rotating barrel electrode; the concentration of copper in the wastewater reduced from an initial value of 100 ppm to

less than 1 ppm. The removal of copper increased with an increase in the applied voltage; however, operating beyond 5 V resulted in the surface passivation of the cathode.

The effect of liquid flow rate and applied voltage on recovery of palladium from hydrochloric acid solution was investigated by Kim *et al.* [49]; they used a modified cyclone reactor that comprised titanium rotating disc electrode, vitreous carbon electrode and saturated calomel reference electrode; compared with laminar flow at 0.6 $m.s^{-1}$, the recovery of palladium increased exponentially under the turbulent flow conditions (3.0 $m.s^{-1}$). Likewise, operating at 3 V, the removal of palladium was twice as fast as that at 1 V. On the whole, 99% of the palladium was recovered from the acidic solution.

A flow-through iron-felt was employed by Grau and Bisang [28] for removal of mercury from wastewater where more than 99.5 % reduction of Hg^{++} was achieved. Winder *et al.* [50] used RVC in a flow-through configuration for the removal of lead; they reported higher removal rates (more than 99 %) at higher liquid flow rates.

Removal of zinc and nickel using porous electrodes has been frequently reported in the literature. Lanza and Bertazzoli [37] used RVC as cathode for the removal of zinc from an aqueous zinc chloride medium under batch recycle operation; reduction of zinc from an initial value of 50 to a final value of 0.1 $mg.dm^{-3}$ was reported. On the other hand, in his study, using a graphite bed electrode, Simonsson [35] reported 99 % reduction of zinc from a zinc sulfate medium. Njau and co-workers [51] studied the removal of nickel using a variety of electrode materials, such as a bed of graphite particles, RVC, and a stack of expanded nickel sheets; it was concluded that high porosity electrodes were advantageous for removal of nickel. Ohran *et al.* [52] employed a rotating packed bed cell of metal granules for the removal of nickel ions. A 90 % reduction in nickel concentration was reported, and was attributed to the high surface area of the electrode and improved mass transfer due to the rotation of the electrode. This brief literature survey shows that porous electrodes have been successfully used, in a variety of configurations, to remove heavy metals from wastewater. That is why porous electrodes were used in the present study to remove Zn^{++} and Ni^{++} from wastewater.

3. Experimental

3.1. Experimental Apparatus

The experimental apparatus used in the present study is shown in Figure 3.1. The electrochemical cell and holding tank were constructed from PVC. The apparatus operated in batch recirculation. Wastewater pumped from the holding tank would pass through a heat exchanger and enter the top of the electrochemical cell; after flowing through the porous electrodes, the wastewater would exit the electrochemical cell via orifices at the bottom and return to the holding tank.

The liquid flow rate was varied both in the laminar and turbulent flow regimes. The characterization of the flow regime, either laminar (0.00471 and 0.00943 $m3.m^{-2}.s^{-1}$) or turbulent (0.01414, 0.01886 and 0.02357 $m3.m^{-2}.s^{-1}$), was based on the diameters of the electrochemical cell and the orifices drilled at the bottom of the cell. The electrochemical cell had an internal diameter of 15 cm and a height of 33 cm. Eight orifices, each having a diameter of 0.5 cm, were drilled at the bottom of the electrochemical cell. Sample calculation to determine the orifice diameter is provided in Appendix A. The electrochemical cell was considered as a short pipe; for internal flow in this pipe, the transition from laminar to turbulent region occurred within the typical Reynolds number range of 2100 to 4000. Sample calculations for different volumetric liquid fluxes and Reynolds numbers are also provided in Appendix A.

To maintain a certain liquid head within the electrochemical cell, different arrangements of the orifices were used with respect to laminar and turbulent flow regimes; the orifices were either plugged at alternating locations, or completely left open as shown in Figure 3.2 (a-d) A variable area direct reading flow meter (Model F-45750- LHN 12, Fabco Plastics, Maple, Ontario) with a range of 1 to 10 (U.S) gallons /min was used for liquid flow measurement.

The heat exchanger was used to maintain the temperature of the wastewater around 25°C for all runs. A by-pass line leading back to the holding tank was used to provide for

Figure 3.1: Schematic diagram of the experimental apparatus for electrochemical treatment of simulated wastewater (Dashed (--) lines represent the wires connecting anode and cathode to direct current power supply)

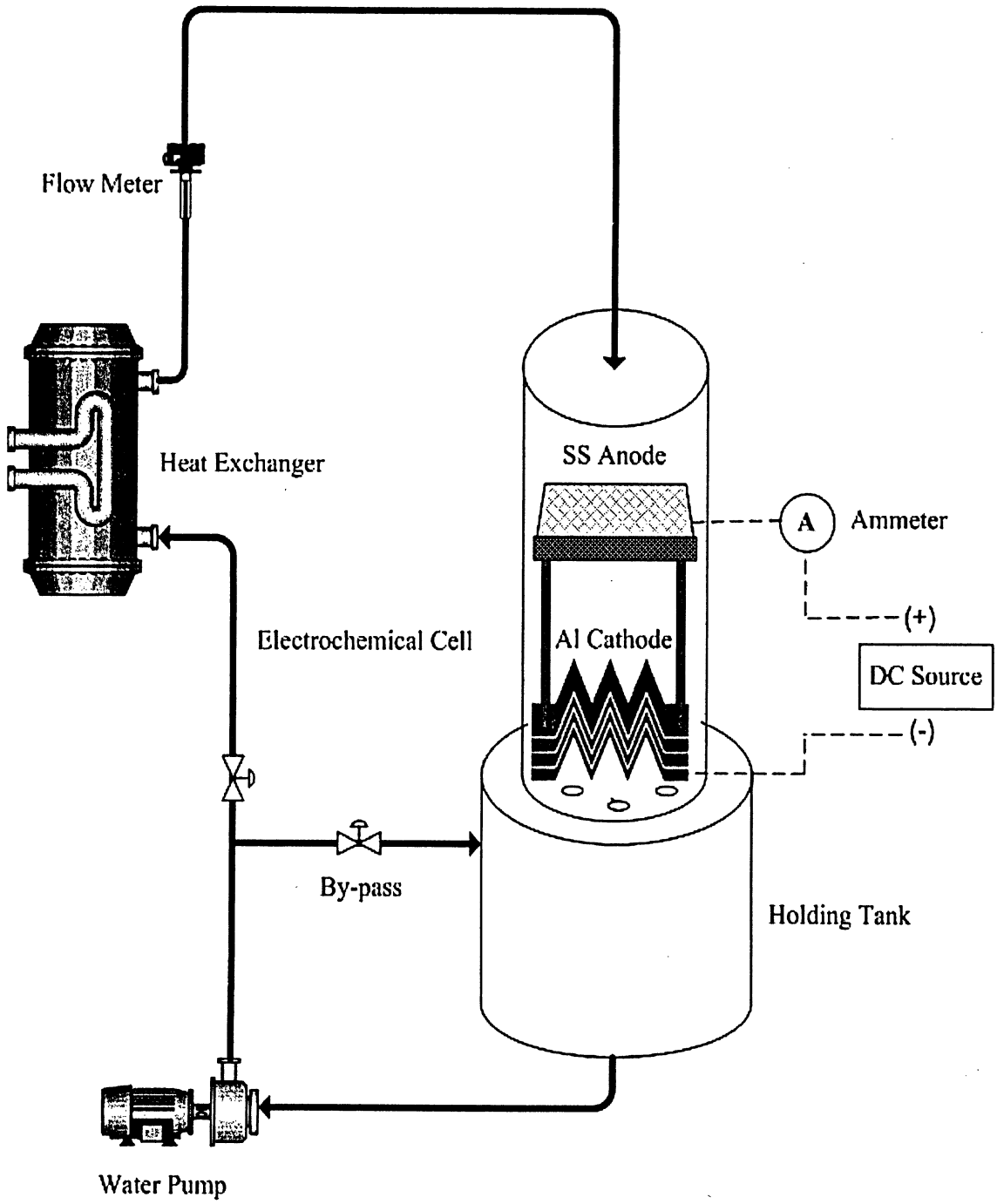

Figure 3.2: Different arrangements of the orifices at the bottom of the electrochemical cell with respect to different volumetric liquid fluxes (dark and light colored circles show closed and open orifices, respectively)

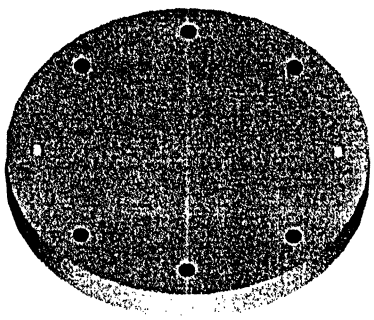

Fig 3.2(a): Arrangement for volumetric liquid fluxes of 0.00471 and 0.00943 $m^3.m^{-2}.s^{-1}$. (Laminar)

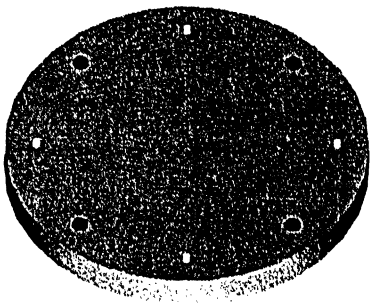

Fig 3.2(b): Arrangement for volumetric liquid flux of 0.01414 $m^3.m^{-2}.s^{-1}$. (Turbulent)

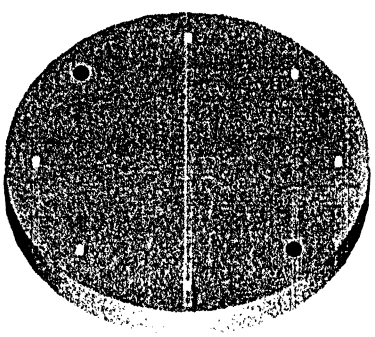

Fig 3.2(c): Arrangement for volumetric liquid flux of 0.01886 $m^3.m^{-2}.s^{-1}$. (Turbulent)

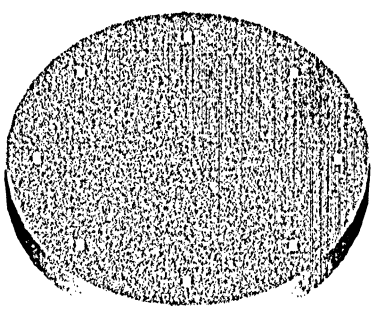

Fig 3.2(d): Arrangement for volumetric liquid flux of 0.02357 $m^3.m^{-2}.s^{-1}$. (Turbulent)

efficient mixing of wastewater in the holding tank as well as to regulate the liquid flow rate.

A DC Electro power supply (Model 612 T) was used to supply a voltage from 5 to 25 V. A Simpson ammeter (Model 373) was connected in series for current measurement.

3.1.1. Electrochemical Cell

In the present study, porous electrodes were used in the electrochemical cell. The materials chosen for the anode and the cathode were stainless steel (SS) and aluminum, respectively. The choice was made because of the cheap availability and superior electrowinning characteristics of these materials [5].

A porous stainless steel anode was constructed in-house. A 4-mesh size AISI 316 SS and AISI 316 SS netting were used. The netting was supplied by Microwire, Toronto, Ontario. Sixteen layers of the stainless steel netting were sandwiched between the two stainless steel meshes. The resulting sandwich was held in place by stainless steel tie wires at its four corners and was compressed to a thickness of 1.5 cm; the stainless steel tie wire extending from the top of the anode served as current feeder., and was connected to the power supply The SS anode had a specific surface area of 16.75 cm^{-1} (see Appendix A for sample calculations) and it rested on the two 10 cm long hollow cylindrical PVC supports extending from the top of the cathode.

Initially, aluminum foam (ERG Aerospace and Materials, CA), with a grade of twenty pores per inch (20 ppi), and having a specific surface area of 10.67 cm^{-1}, was used as cathode. However, after just three experimental runs, it became brittle and started to disintegrate. Therefore, a porous aluminum cathode was constructed in-house. Increased surface area and better resistance to higher flow rates and voltages were the main design considerations for the new electrode. Four aluminum plates (Metal Supermarket, Toronto) were perforated with a 1 mm bit; each plate was 21 cm long, 9 cm wide and 0.08 cm thick, and had eighty four holes, with each hole having a diameter of 0.1 cm. The perforated plates were then corrugated at an angle of 60° (see Figure 3.3).The plates were

stacked together to form a cathode that had an area of 1507 cm^2 The cathode was connected to the power supply using an aluminum wire; two 1 cm long PVC rings separated one corrugated aluminum plate from the other.

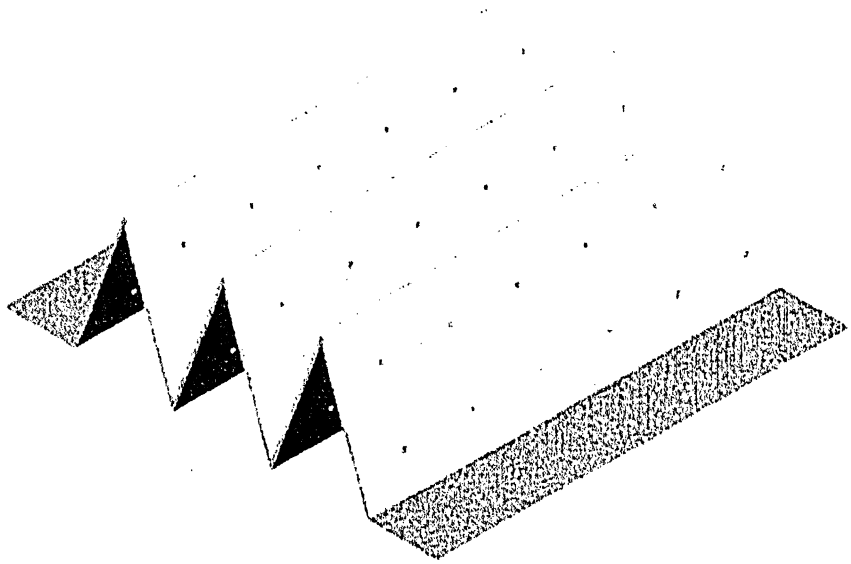

Figure 3.3: Corrugated aluminum plate with perforations

3.2. Experimental Procedure

3.2.1. Cleaning Prior to Experimental Runs

Prior to any experimental run, the apparatus was cleaned with distilled water; distilled water was flushed through the system for at least 2 hours and then drained.

Electrodes were also cleaned prior to any run. The stainless steel anode was brushed with stainless steel brush to remove any loose deposits; it was then rinsed with distilled water and allowed to dry.

The cathode was stripped of any deposits by soaking it in 1:1 molar aqueous nitric acid bath for 60 minutes; it was then washed with tap water and rinsed with distilled water.

All glassware was cleaned by using mild detergent, followed by at least three rinses with tap water, and then a final rinse with distilled water.

3.2.2. Preparation of Simulated Wastewater

In the present study, zinc sulfate heptahydrate and nickel sulfate hexahydrate (J.T. Baker) were used to make the simulated wastewater with zinc and nickel ion concentrations of 20 ppm each. Potassium sulfate (J.T. Baker) was used as supporting electrolyte with a concentration of 500 ppm. The volume of simulated wastewater used for any experimental run was 35 liters.

To prepare the simulated wastewater with desired concentration of metal ions and electrolyte, a 4 liter Erlenmeyer flask was used. Approximately two liters of distilled water was added to the flask. 3.076 g of zinc sulfate heptahydrate, 3.172 g of nickel sulfate hexahydrate, and 17.5 g of potassium sulfate were weighed using an electronic balance (Scientech Inc., Boulder, Colorado) and added to the flask. The contents were then stirred to dissolve the solutes, and added to 33 liters of distilled water in the holding tank.

3.2.3. Electrochemical Treatment

The simulated wastewater was added to the holding tank and the pump was turned on. The water was allowed to flow through the apparatus for at least 5 minutes to ensure complete mixing of metal ions and electrolyte. The water valves were adjusted to maintain a desired liquid flow rate, and once the electrodes were completely submerged, the power supply was turned on and its knob was adjusted to supply a desired voltage. The electrochemical treatment time for any run was 48 hours.

Samples were drawn from the holding tank at regular time intervals of 0, 4, 8, 24, 28, 32 and 48 hours. A100 ml beaker (VWR, Inc) was used to take grab samples of wastewater from the holding tank. The samples were immediately analyzed for pH and metal ions concentration Likewise, the current and temperature of the wastewater were measured at the aforementioned time intervals. At the end of 48 hours of electrochemical treatment,

the wastewater was drained out from the bottom of the holding tank and the electrodes were taken out from the electrochemical cell for cleaning.

In the first phase of experimental runs, the volumetric liquid flux was kept constant at 0.02357 $m^3.m^{-2}.s^{-1}$, and the applied voltages were varied from 5 to 25 V; in second phase, the applied voltage was kept constant at 10 V, and the volumetric liquid fluxes were varied from 0.00471 to 0.02357 $m^3.m^{-2}.s^{-1}$ For all runs, the temperature of the simulated wastewater was maintained at 25°C and the pH was maintained between 5.6-6.0.(a summary of experimental runs is provided in Appendix B) A detailed description of the activities performed during any experimental run is provided in the following sections.

3.2.3.1. Temperature, Current and pH Measurements

During any experimental run, the temperature of the simulated wastewater was measured using glass thermometer (VWR, Inc). The thermometer was dipped in the holding tank for 10 seconds and the temperature was recorded immediately. If the recorded temperature was less than 25°C, the flow of the cooling water into the heat exchanger was decreased, and vice versa.

Similarly, the current was measured, at regular time intervals, using an ammeter. For all experimental runs, the current decreased during the first three to four hours of electrochemical treatment because of the reduction of the Ni^{++} and Zn^{++}. However, as the concentration of the metal ions in the bulk electrolyte decreased, the current attained a stable value.

The pH of the sample was measured with a Corning 220 pH meter. In accordance with the manufacturer's manual, the pH meter was calibrated on daily basis using buffers of 4 and 7. For all runs, during the first eight hours of electrochemical treatment, the pH of the wastewater was measured after every hour. Adjustment to the pH of the simulated wastewater, between 5.6 and 6.0, was done by adding 1.0 M potassium hydroxide (J.T. Baker) and 1.0 M sulfuric acid (Merck KGaA). For all runs, typically 20-25 ml of potassium hydroxide and 5-6 ml of sulfuric acid were used.

3.2.3.2. Analysis of Zn^{++} and Ni^{++}

The concentrations of Zn^{++} and Ni^{++} in the simulated wastewater were measured using a spectrophotometer (Model 975 PM, Orbeco-Hellige, Farmingdale, New York). The wastewater samples, which were to be analyzed for Zn^{++} and Ni^{++} concentration, were prepared according to standard methods (zincon method and dimethylgloxime method for Zn^{++} and Ni^{++}, respectively) provided in the manufacturer's literature (Orbeco-Hellige). For both methods, 10 ml of wastewater sample was put in a separate beaker and diluted with 90 ml of distilled water. Three glass tubes (provided with spectrophotometer) were filled with 10 ml of diluted wastewater sample each. One of these tubes was used as reference or blank tube, and the other two were used to prepare sample tubes for detecting zinc and nickel.

In zincon method, the sample tube was prepared by adding crushed zinc tablet (VWR, Inc) to one of the tubes containing diluted wastewater sample. The sample tube for zinc was then left aside for 5 minutes for the contents to dissolve. Similarly, the sample tube to be used in the dimethylgloxime method was prepared by adding, 2 ml of ammonium citrate (VWR, Inc), 1 ml of iodine (VWR, Inc) 4 ml of ammonium hydroxide (VWR, Inc) and 18 drops of dimethylgloxime (VWR, Inc) to one the tubes containing diluted wastewater samples. The sample tube for nickel was then left aside for 7 minutes for solutions to react completely.

The spectrophotometer had a detection range of 0 to 4 mg/l^{-1} for zinc at a wavelength of 640 nm, whereas the detection range for nickel was 0 to 12 mg/l^{-1}at a wavelength of 528 nm. To measure metal ions concentration, first, the knob of the spectrophotometer was set to a specific wavelength and the reference tube was inserted. The spectrophotometer would beep after it had finished analyzing the reference tube. Then the sample tube was inserted, and after 5 seconds, the concentration of the metal ion could be read from the L.C.D (liquid crystal display) screen of the spectrophotometer. This measured concentration of metal ion, either zinc or nickel, was for the diluted wastewater sample and was multiplied by 10 to find actual concentration of metal ion in the original wastewater sample.

3.3. Viscosity and Density Calculations

The dynamic viscosity of the simulated wastewater and density were assumed to be the same as calculated by Mitzakov [15] for the simulated wastewater having 20 ppm of Zn^{++}, 20 ppm of Ni^{++}, and 500 ppm of potassium sulfate. Calculation details of the method adopted by Mitzakov are provided in Appendix A.

3.4. Data Analysis

Uncertainties associated with the concentrations of zinc and nickel were calculated from multiple readings; all outlier values were discarded and average and standard deviations associated with zinc and nickel were calculated from the remaining data [53]. Similarly, the uncertainties associated with the average mass transfer coefficient were determined from the method of Kline and McClintock [54]

4. Results and Discussion

4.1. Effect of Applied Voltage

4.1.1. Effect of Applied Voltage on Removal of Zn^{++} and Ni^{++}

Figure 4.1 presents the effect of the applied voltage on the reduction of zinc ions for a volumetric flux of 0.02357 $m^3.m^2.s^{-1}$ in the turbulent region; it shows that when the applied voltage to the electrochemical cell was increased, the removal of Zn^{++} increased as well. The effect of applied voltage became distinct after just 8 hours of electrochemical treatment; the percent removal of Zn^{++} increased from 71 % at 5 V to 91 % at 25 V. However, operating at the higher voltages (from 10 to 25 V), there was not much difference (only 2 %) as to removal of zinc ions at the end of 48 hours of electrochemical treatment.

In the present study, the fractions of Zn^{++} and Ni^{++} remaining in the electrolyte were found to have a square-root relationship with time (Fig. 4.2). The governing equation (eq. 4.1) describing the reduction of Zn^{++} and Ni^{++} was extracted from an analogous model in which the diffusion of species from a stirred solution of limited volume varied as the square root of time [55]:

$$\ln\left(\frac{C_t}{C_o}\right) = -kt^{1/2} \tag{4.1}$$

where the ratio (C_t / C_o) represents the fraction of metal ions remaining in the electrolyte, C_t is the concentration of the metal ions at any given time t, C_o is the initial concentration of the metal ions, and k is the apparent rate constant for the reduction of metal ions.

Figure 4.2 presents a semi-log plot of the fractional zinc ion concentration versus square root of time; the apparent rate constants for Zn^{++}, obtained from the slopes of the corresponding regression lines, are reported in Table 4.1

Figure 4.1: Effect of applied voltage on Zn^{++} removal during electrochemical treatment using porous corrugated aluminum cathode and SS anode at volumetric liquid flux of 0.02357 $m^3.m^{-2}.s^{-1}$ (T = 25°C; pH = 5.6-6; I = 0.044, 0.155, 0.260, 0.360 and 0.470 A at applied voltages of 5, 10 ,15 ,20 and 25V, respectively)

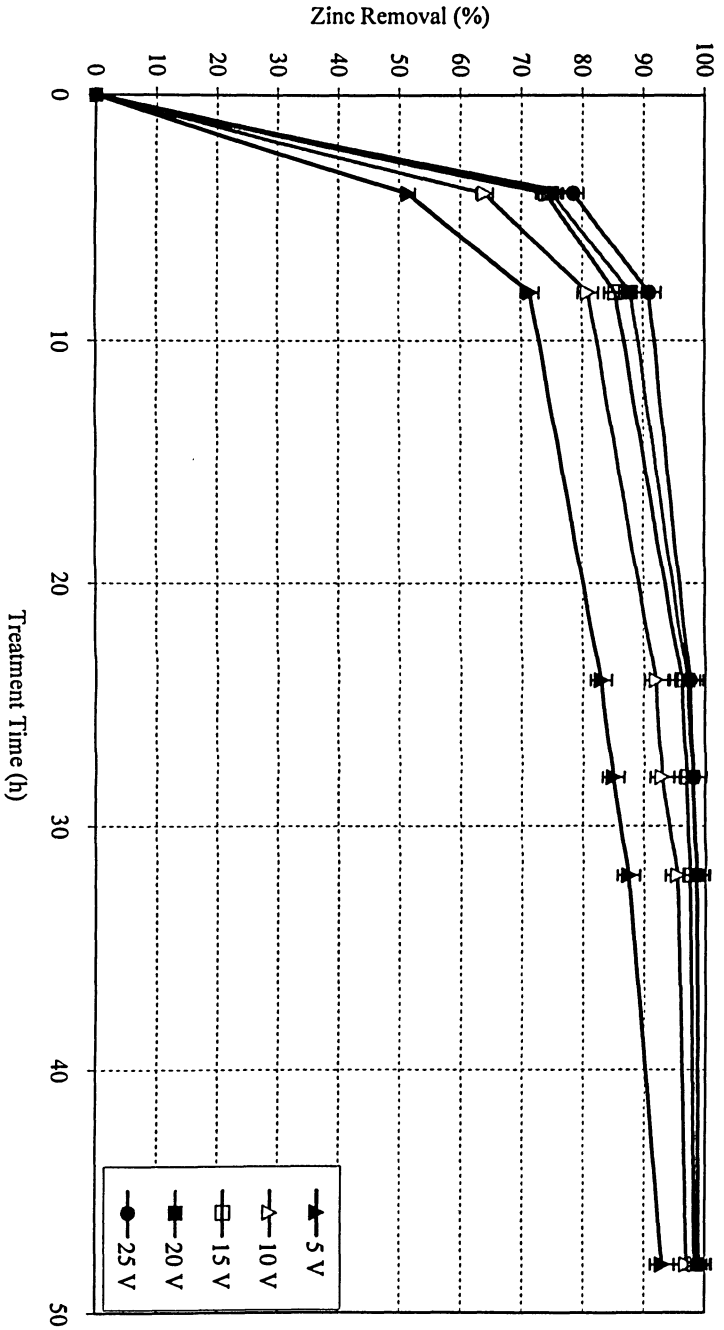

Figure 4.2: Linear regression for Zn^{++}: Effect of applied voltage during electrochemical treatment using porous corrugated aluminum cathode and SS anode at volumetric liquid flux of 0.02357 $m^3.m^{-2}.s^{-1}$ (T = 25°C; pH = 5.6-6; I = 0.044, 0.155, 0.260, 0.360 and 0.470 A at applied voltages of 5, 10 ,15 ,20 and 25V, respectively). Solid line is linear regression

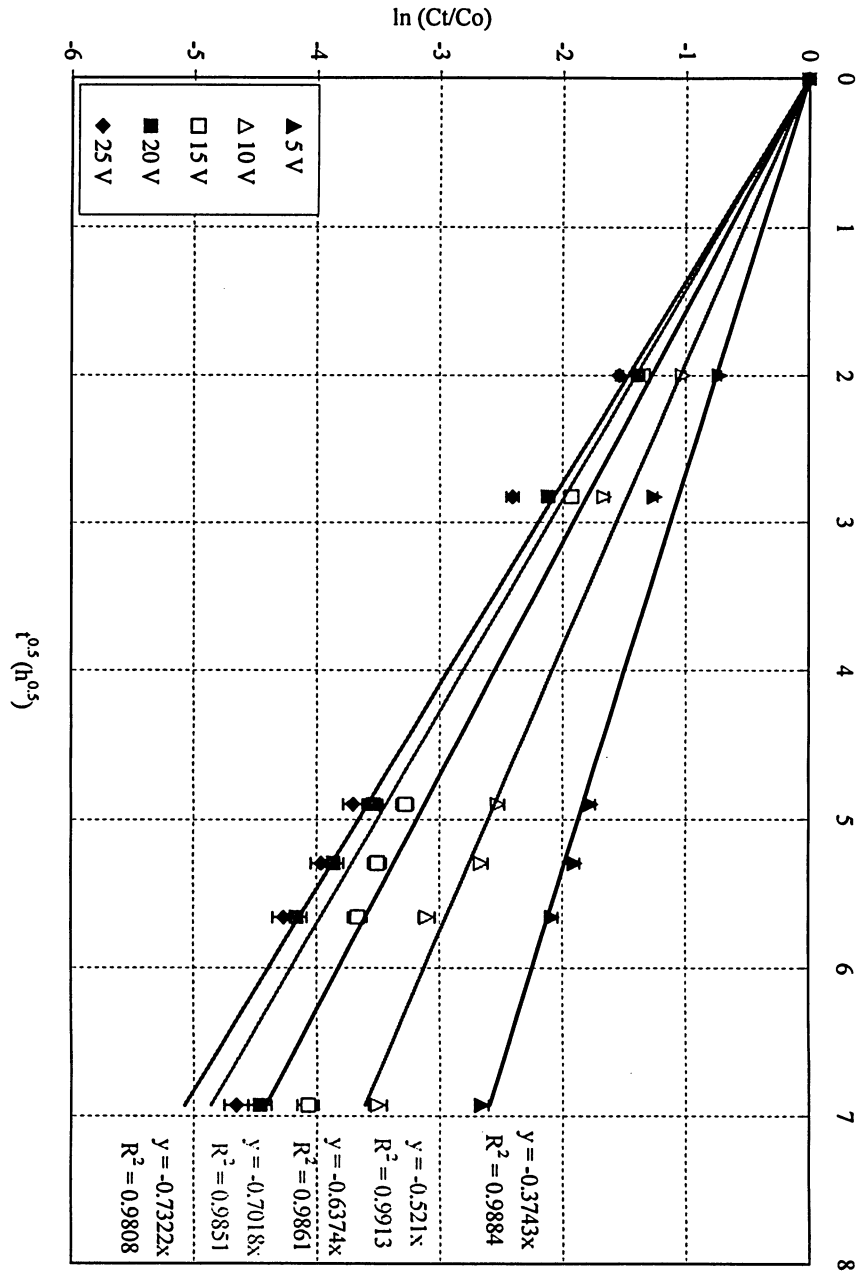

The results for nickel ions removal are presented in Figure 4.3. In contrast to Zn^{++}, a different trend was observed in case of Ni^{++} removal. At the end of 48 hours of electrochemical treatment, the percent removal of nickel ions increased from 66 % at 5 V to 77.5 % at 10 V. However, further increase in the applied voltage resulted in the decrease of nickel ions removal- beginning from 72 % at 15 V, it finally decreased to 56 % at 25 V. Figure 4.4 shows a semi-log plot of the fractional nickel ion concentration versus square root of time; a summary of the apparent rate constants, which were obtained from the slopes of corresponding regression lines, is presented in Table 4.1.

4.1.2. Effect of Applied Voltage on Apparent Rate Constants

Table 4.1 shows the effect of applied voltage on apparent rate constants for nickel and zinc. The rate constants for zinc increased with corresponding increase in the applied voltage. For nickel, the rate constant initially increased for applied voltages of 5 to 10 V; however; it started decreasing again after an applied voltage of 15 V, and kept decreasing with further increase in the voltage.

Table 4.1: Apparent rate constants for Zn^{++} and Ni^{++}

Applied voltage (V)	Apparent rate constant, k ($s^{-0.5}$)	
	Zn^{++}	Ni^{++}
5	6.24E-03	2.60E-03
10	8.68E-03	3.53E-03
15	10.6E-03	2.91E-03
20	11.7E-03	2.44E-03
25	12.2E-03	2.02E-03

From the discussion in the preceding sections, two anomalies are found with respect to removal of nickel and zinc ions from the electrolyte:

Figure 4.3: Effect of applied voltage on Ni^{++} removal during electrochemical treatment using porous corrugated aluminum cathode and SS anode at volumetric liquid flux of 0.02357 $m^3.m^{-2}.s^{-1}$ (T = 25°C; pH = 5.6-6; I = 0.044, 0.155, 0.260, 0.360 and 0.470 A at applied voltages of 5, 10 ,15 ,20 and 25V, respectively)

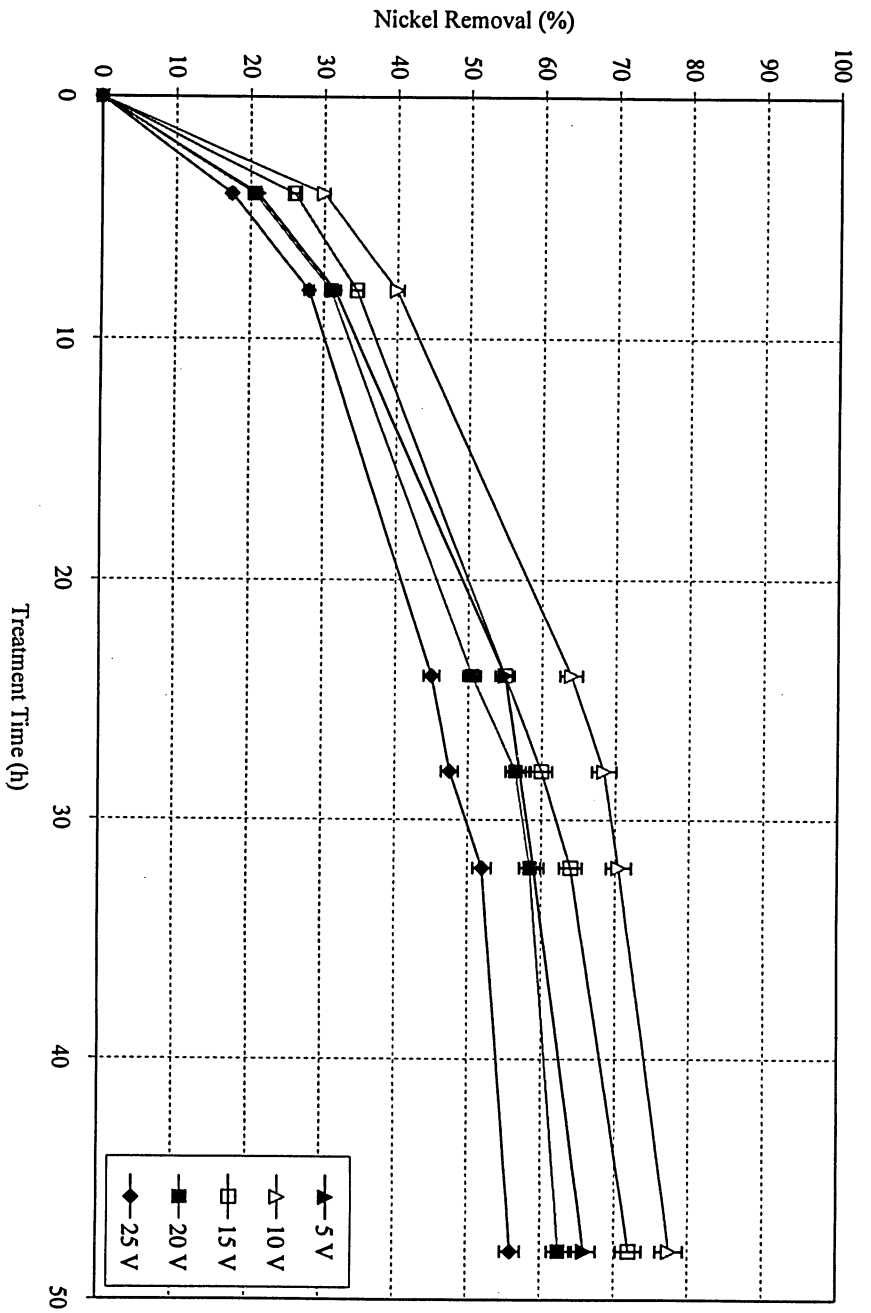

Figure 4.4: Linear regression for Ni^{++}: Effect of applied voltage during electrochemical treatment using porous corrugated aluminum cathode and SS anode @ volumetric liquid flux of 0.02357 $m^3.m^{-2}.s^{-1}$ (T = 25°C; pH = 5.6-6; I = 0.044, 0.155, 0.260, 0.360 and 0.470 A at applied voltages of 5, 10 ,15 ,20 and 25V, respectively). Solid line is linear regression.

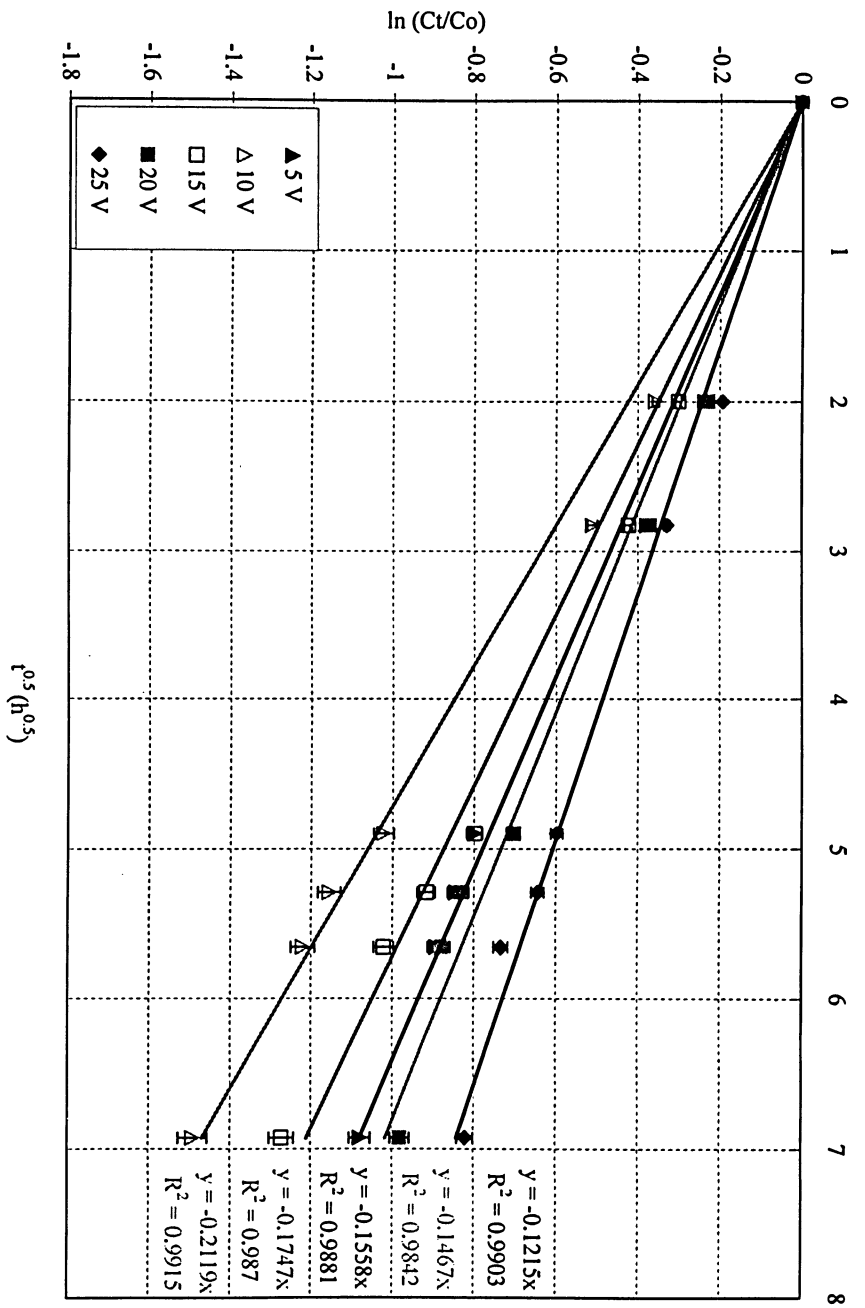

- The standard reduction potential for Ni^{++} is -0.23 V (Eq. 2.5), which is higher than that of -0.76 V for Zn^{++} (Eq.2.4). At the beginning of present study, it was assumed that nickel ions would be removed more readily from the electrolyte than zinc ions. Nevertheless, when both nickel and zinc ions were present, the deposition of zinc ions increased. However, this is not a new phenomenon; in the literature, it has been frequently referred to as anomalous co-deposition [56-61].
- The deposition of Zn^{++} increased with a corresponding increase in the applied voltage. The Ni^{++} deposition followed a different path; it initially increased up to an applied voltage of 10 V, and started to decline again after an applied voltage of 15 V; this apparent anomaly may be addressed against the backdrop of excessive precipitation of nickel ions as Ni $(OH)_2$ when operating at higher voltages (15 V and above).

A brief discussion of the phenomena working behind the aforementioned anomalies is provided as an aside in the following sections.

4.1.3. Applied Voltage and Anomalous Co-deposition

The term "anomalous co-deposition" refers to the phenomenon occurring during the electrodeposition of two or more metals, in which the less noble metal deposits more readily than the more noble metal.

Anomalous co-deposition of metals is a complex phenomenon; though many attempts have been made to explain it, there is still no universally acceptable theory. Perhaps the earliest theory to explain the phenomenon of anomalous co-deposition was propounded by Brenner [56]. In his theory, known as addition agent theory, Brenner explained the formation of an agent due to cathodic reaction occurring during electrodeposition, which hinders the deposition of more noble metal. The formation of the agent is deemed to occur only when the current density is adequately high to raise the pH of the cathode diffusion layer appreciably.

According to a different theory proposed by Dahms and Croll [57], anomalous co-deposition occurs because of the formation of metallic hydroxides layer on the cathode, which suppresses the deposition of more noble metal. The formation of metallic hydroxides occurs because of the excessive evolution of hydrogen and hydroxyl ions. In their study, Dahms and Croll [57] used an iron-nickel alloy system, and it was believed that the formation of ferrous hydroxide layer blocked nickel discharge, whereas iron discharged readily through this layer. To further expound their theory, a model was developed to demonstrate that the electrode surface pH could rise to as much as 9.0 for an iron-nickel system having a bulk pH of 2.5. Other researchers, Highashi *et al.* [36] and Fukushima *et al.* [58], have validated through experimentation the hydroxide suppression of the more noble metal, for a zinc-cobalt and zinc-nickel systems, respectively.

Another theory, which is based on the kinetic mechanisms involved during co-deposition of metals, has also been developed. According to this theory, metal intermediates adsorbed on the cathode surface act as catalysts for the deposition of less noble metals. The studies that substantiate this theory include zinc-nickel systems in sulfate medium [59] or chloride medium [60].

In the present study, as there was no means of either measuring the surface pH of the cathode or of determining the presence of intermediate adsorbates, results were compared with similar studies done by other investigators; for zinc-nickel system in sulfate medium, Ishihara *et al.* [61] reported the formation of zinc hydroxide film, through which a preferential deposition of zinc ions was observed. In their study, the pH of the electrolyte was 2.0 and the zinc hydroxide film formation was supposed to be caused by rise in the pH near the cathode surface. In the present study, the pH of the electrolyte was maintained between 5.6 and 6.0. Thus, compared with their study, there was greater probability of the formation of zinc hydroxide in the present study. Therefore, the theory proposed by Dahms and Croll [57] appears to provide a reasonable explanation vis-à-vis the anomalous co-deposition Zn^{++} and Ni^{++} observed in the present work.

4.1.4. Applied Voltage and Precipitation of Metal Ions

In electrochemical treatment, precipitation of metal ions depends on the pH of the bulk electrolyte. The complex reactions occurring in an electrochemical cell alter the pH of the electrolyte to a great extent. During the electrodeposition of metals, besides the reduction of metal ions at the cathode, many side reactions occur both at the anode and cathode, and in the bulk solution. These reactions may include the electrolysis of water at the anode, decomposition of water at the cathode, the reduction of oxygen at the cathode, the evolution of hydrogen at the cathode, and reaction of metal ions with hydrogen or hydroxide ions [16, 62]. In the present study, in addition to the basic metal reduction reactions (Equation 2.4 and 2.5), the following reactions were believed to have occurred in the electrochemical cell:

The main reaction at the anode under acidic conditions was:

$$2H_2O \longrightarrow O_2 + 4H^+ + 4e^- \qquad (4.2)$$

The decomposition of water occurred at the cathode under alkaline conditions

$$2H_2O + 2e^- \longrightarrow H_2 + 2OH^- \qquad (4.3)$$

The OH^- ions reacted with Zn^{++} and Ni^{++} to form zinc and nickel hydroxide

$$Zn^{++} + 2OH^- \longrightarrow Zn(OH)_2 \qquad (4.4)$$

$$Ni^{++} + 2OH^- \longrightarrow Ni(OH)_2 \qquad (4.5)$$

For all runs, the pH of the bulk electrolyte before electrochemical treatment had an average value of 6.0. With the onset of electrochemical treatment, the pH was observed to decrease, and after one hour of treatment, it had a typical value of 5.5. The anodic reaction (Eq. 4.2) was believed to be responsible for decrease in the pH of the solution.

For the runs that were conducted at 5 and 10 V, pH of the electrolyte had to be adjusted around a value 6.0 after every hour during the first 8 hours of electrochemical treatment. However, a slight increase in pH could be observed after 32 hours of electrolysis time, and it had a typical value of 6.1 at the end of the 48 hours of treatment. The slight increase in pH was due to decomposition of the water at the cathode (Eq 4.3), which became a dominant reaction towards the end of the electrochemical treatment. To verify whether any precipitation of nickel or zinc occurred, 200 ml sample of electrolyte was filtered with Wattman filter paper # 42 at the end of the treatment. No precipitation was observed in the solution, or on the filter paper. Zinc and nickel ion concentrations were also measured in the filtrate. The measured values provided the balance of Ni^{++} and Zn^{++} that remained in the solution.

For runs conducted at 15, 20 and 25 V, the electrolyte began to get milky after just 10 hours of electrochemical treatment, and a slight rise in pH could be observed after 20 hours. It was assumed that due to high applied voltages excessive generation of electrons occurred at the anode (Eq 4.2), and the water decomposition reaction (Eq. 4.3) became dominant in the early stages of electrochemical treatment. The excess OH^-, which were generated at the cathode, readily combined with zinc and nickel ions to form zinc and nickel hydroxides, respectively (Eq. 4.4 & 4.5). In the light of Dahms and Croll's theory of anomalous co-deposition [57], it may be assumed that zinc deposited both as pure metal and as zinc hydroxide, whereas nickel's deposition was further decreased because of the increased precipitation of nickel as nickel hydroxide.

At the end of the electrochemical treatment, the 200 ml sample of the electrolyte was filtered. A light green precipitate could be observed for all runs conducted at 15, 20 and 25 V. The measured concentrations of zinc and nickel ions in the electrolyte, filtrate and precipitate are reported in Table 4.2. It can be seen that at voltages higher than 10 V, increased precipitation of nickel as nickel hydroxide occurred.

The effect of applied voltage on the removal of copper from wastewater was studied by Al-Shammari *et al.* [48], who employed a perforated rotating barrel electrochemical

reactor. A similar trend was observed in their case, when beyond the limiting voltage of 5.5 V, copper started precipitating as Cu $(OH)_2$; a thick layer of Cu $(OH)_2$ was deposited on the cathode. Since they did not control the pH of the electrolyte, surface passivation of the cathode occurred because of increased acidity, which ultimately reduced the removal of copper.

Table 4.2: Effect of applied voltage on metal ions precipitation after 48 hours of electrochemical treatment at 0.02357 $m^3.m^{-2}.s^{-1}$; pH = 5.6-6.0; T=25°C

Applied voltage (V)	Metal ions in the bulk electrolyte ($mg.l^{-1}$)		Metal ions in the filtrate ($mg.l^{-1}$)		Metal ions in the precipitate ($mg.l^{-1}$)	
	Zn^{++}	Ni^{++}	Zn^{++}	Ni^{++}	Zn^{++}	Ni^{++}
5	1.4	6.8	1.4	6.8	Nil	Nil
10	0.6	4.5	0.6	4.5	Nil	Nil
15	0.3	5.6	0.28	0.31	0.02	5.29
20	0.23	7.5	0.19	0.24	0.04	7.26
25	0.20	8.8	0.18	0.21	0.02	8.59

4.2. Effect of Volumetric Liquid Flux

4.2.1. Effect of Volumetric Liquid Flux on Removal of Zn^{++} and Ni^{++}

It was presumed that higher volumetric liquid flux would result in increased mass transfer, thus improving the removal of Ni^{++} and Zn^{++}. To verify this presumption, electrochemical treatment was performed both under laminar and turbulent flow conditions.

The effect of volumetric liquid flux on removal of zinc ions is presented in Fig. 4.5. It is evident from the graph that the reduction of Zn^{++} increased with an increase in the volumetric flux. Within the laminar region, by increasing volumetric liquid flux from 0.00471 to 0.00943 $m^3.m^{-2}.s^{-1}$, the final reduction of Zn^{++} increased almost by 5 %. However, the effect of volumetric flux became more pronounced in the turbulent region, from 0.01414 to 0.02357 $m^3.m^{-2}.s^{-1}$. During the first 8 hours of electrochemical treatment, the reduction of Zn^{++} increased from 58 % at 0.00471 $m^3.m^{-2}.s^{-1}$ to 81% at 0.02357 $m^3.m^{-2}.s^{-1}$, while after 48 hours of electrochemical treatment, the removal of Zn^{++} was 97 % at 0.02357 $m^3.m^{-2}.s^{-1}$ compared to 84% at 0.00471 $m^3.m^{-2}.s^{-1}$.

Figure 4.6 proves again the square-root dependence of reduction of Zn^{++} on time; the apparent rate constants for Zn^{++}, obtained from the slopes of the corresponding regression lines, are reported in Table 4.3.

The results for nickel ions removal are shown in Figure 4.7. It can be seen that the removal of nickel gradually increased with an increase in the volumetric liquid flux; at the end of 48 hours of treatment, the final removal of Ni^{++} increased from 60% at 0.00471 $m^3.m^{-2}.s^{-1}$ to 77.5 % at 0.02357 $m^3.m^{-2}.s^{-1}$;

Figure 4.8 proves the square root relationship described earlier; apparent rate constants for Ni^{++}, which were obtained from the slopes of the corresponding regression lines, are reported in Table 4.3. The bar graph (Figure 4.9) compares the effects of volumetric liquid flux on the removal of Zn^{++} and Ni^{++} , both under laminar and turbulent flows; it also shows the effects described in the preceding lines.

Figure 4.5: Effect of volumetric liquid flux on Zn^{++} removal during electrochemical treatment using porous corrugated aluminum cathode and SS anode at an applied voltage of 10 V (T = 25°C; pH = 5.6-6; I = 0.155 A)

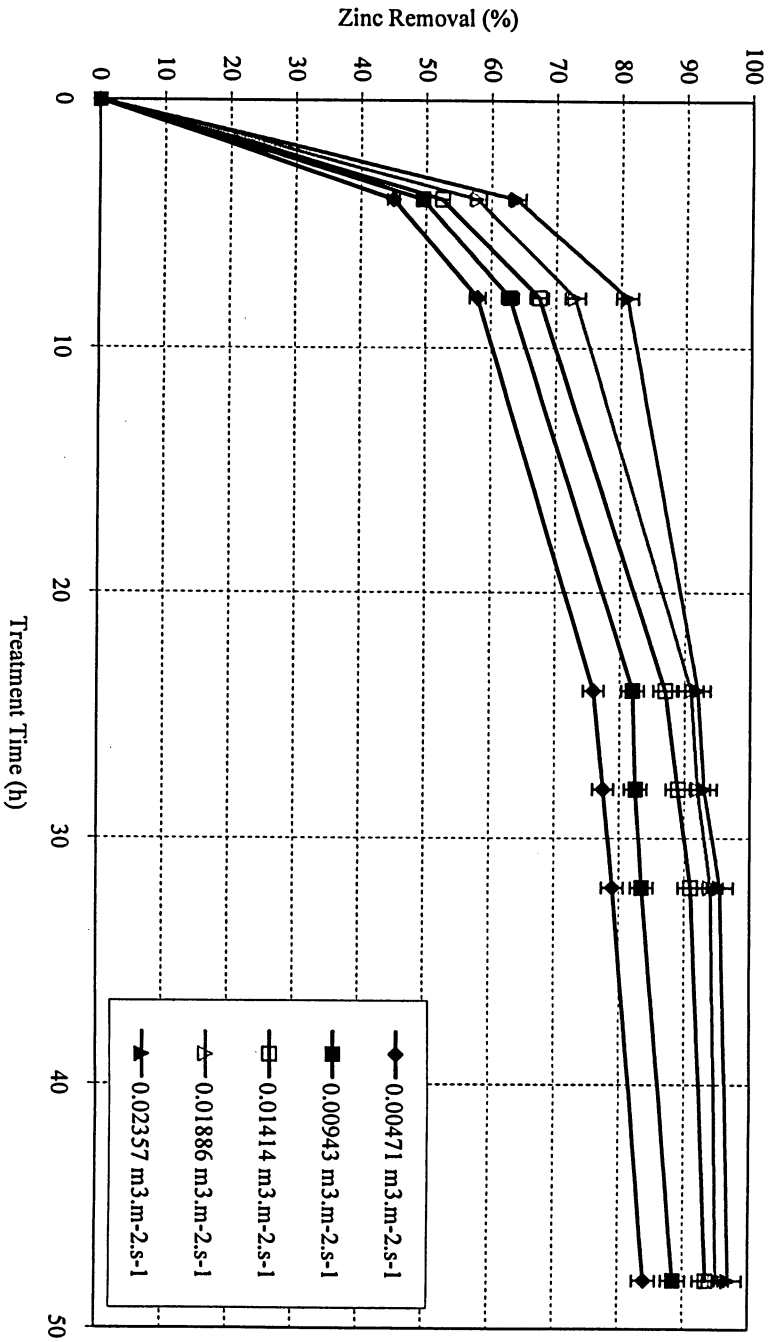

Figure 4.6: Linear regression for Zn^{++}: Effect of volumetric liquid flux during electrochemical treatment using porous corrugated aluminum cathode and SS anode at an applied voltage of 10 V (T = 25°C; pH = 5.6-6; I = 0.155 A). Solid line is linear regression

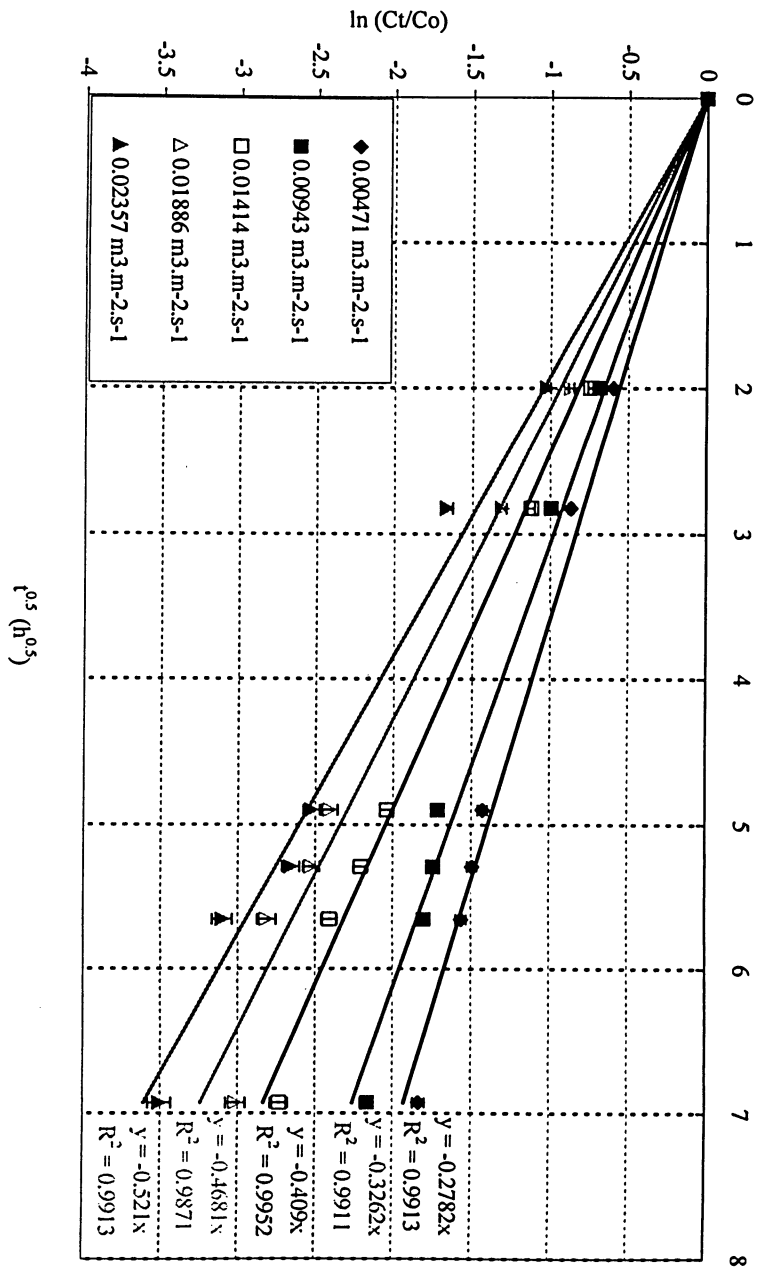

Figure 4.7: Effect of volumetric liquid flux on Ni^{++} removal during electrochemical treatment using porous corrugated aluminum cathode and SS anode at an applied voltage of 10 V (T = 25°C; pH = 5.6-6; I = 0.155 A)

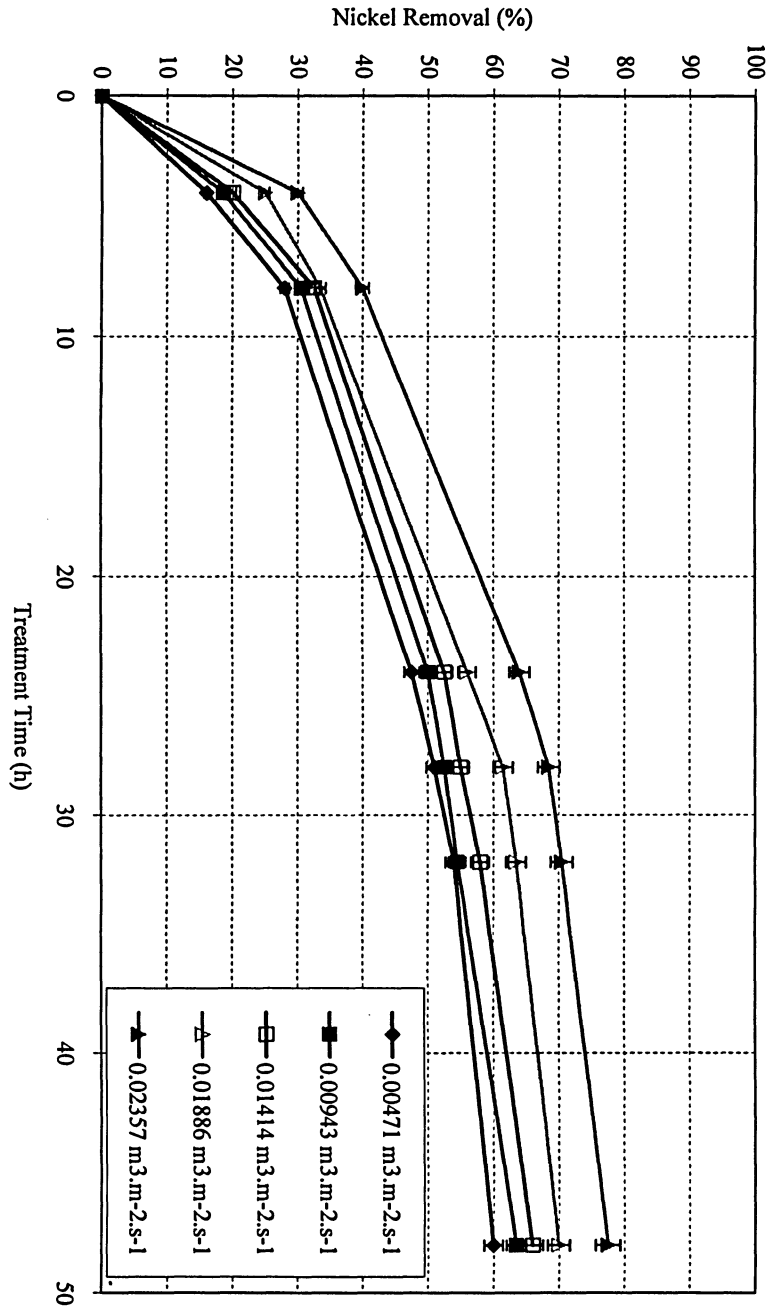

Figure 4.8: Linear regression for Ni^{++}: Effect of volumetric liquid flux during electrochemical treatment using porous corrugated aluminum cathode and SS anode at an applied voltage of 10 V (T = 25°C; pH = 5.6-6; I = 0.155 A). Solid line is linear regression

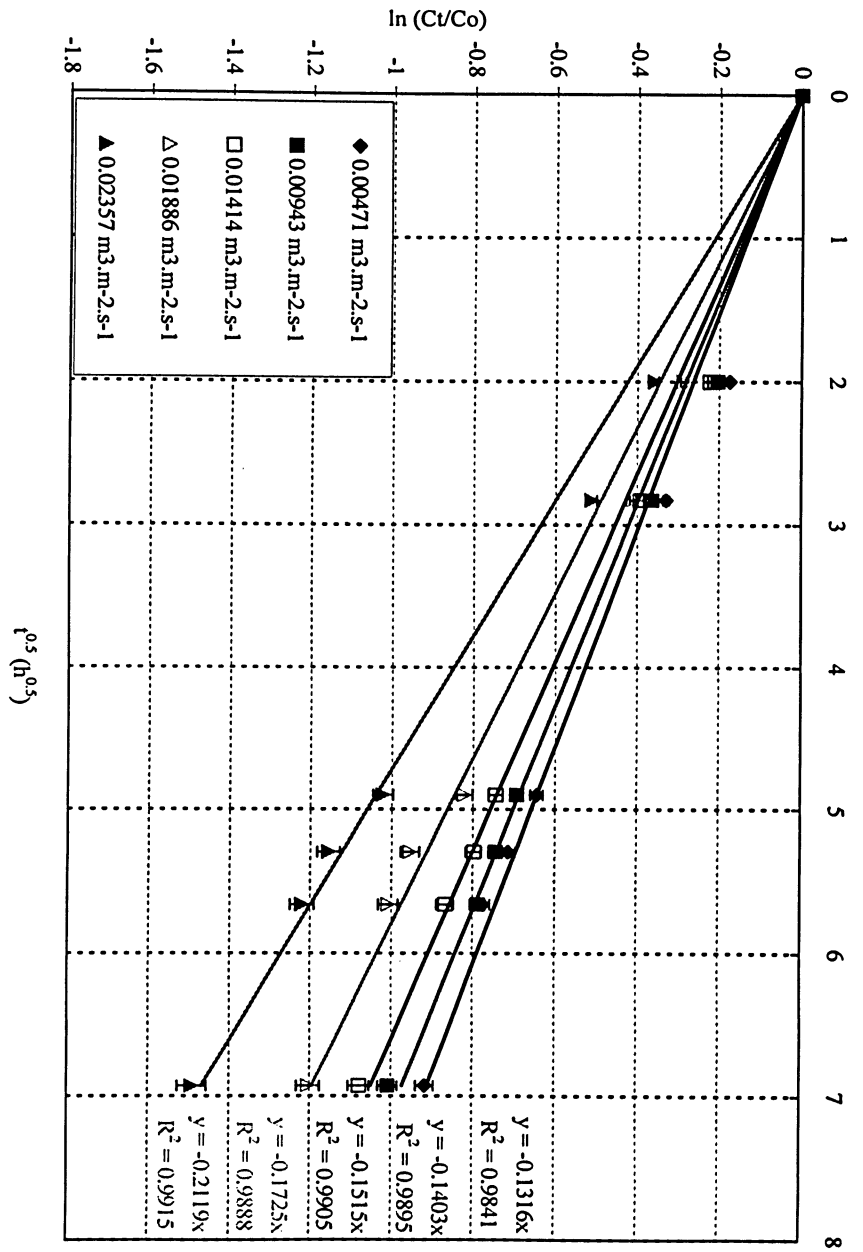

Figure 4.9: Comparison between Zn^{++} and Ni^{++} removal in the laminar and turbulent flow regimes during electrochemical treatment using porous corrugated aluminum cathode and SS anode at an applied voltage of 10 V (T = 25°C; pH = 5.6-6; I = 0.155 A)

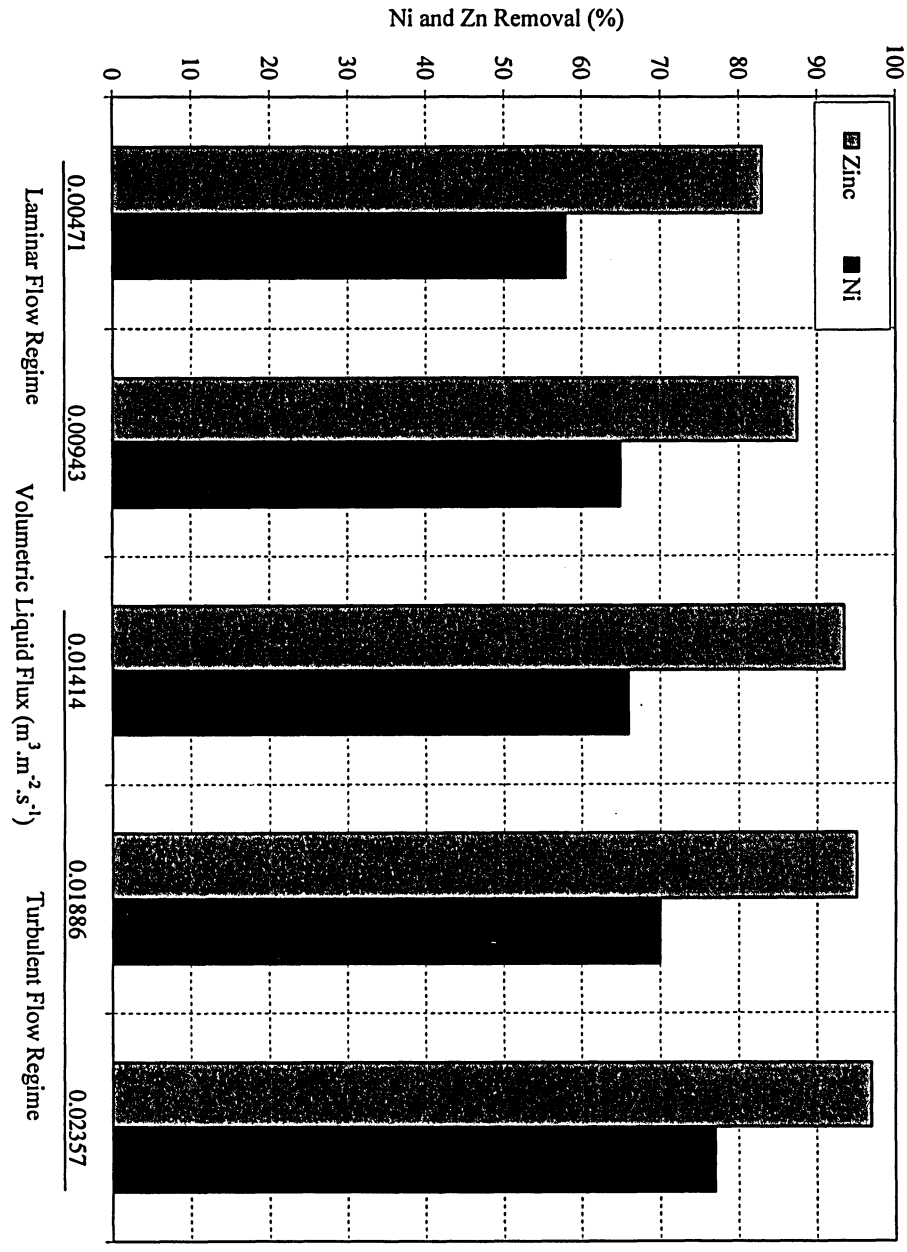

4.2.2. Effect of Volumetric Liquid Flux on Apparent Rate Constant (k) and Mass Transfer Coefficient (k_m)

In the present study, the average mass transfer coefficients were obtained through concentration decay measurements of Zn^{++} and Ni^{++}. Sample calculations to determine average mass transfer coefficient and the uncertainties associated with it, both for nickel and zinc, are provided in Appendix A. Figure 4.10 compares mass transfer coefficients obtained for Zn^{++} and Ni^{++} from laminar to turbulent flow regimes. Similarly, Table 4.3 presents the effects of volumetric liquid flux, both in the laminar and turbulent regions, on apparent rate constants and mass transfer coefficients for Zn^{++} and Ni^{++}.

Table 4.3: Apparent rate constants (k) and mass transfer coefficients (k_m) for Zn^{++} and Ni^{++} (T = 25°C; pH = 5.6-6.0; applied voltage = 10 V)

Flow regime	Volumetric liquid flux ($m^3.m^{-2}.s^{-1}$)	k ($s^{-0.5}$)		k_m ($m.s^{-1}$)	
		Zn^{++}	Ni^{++}	Zn^{++}	Ni^{++}
Laminar	0.00471	4.64E-03	2.19E-03	2.41E-06	1.22E-06
	0.00943	5.44E-03	2.34E-03	2.83E-06	1.33E-06
Turbulent	0.01414	6.82E-03	2.52E-03	3.52E-06	1.44E-06
	0.01886	7.80E-03	2.87E-03	3.83E-06	1.58E-06
	0.02357	8.68E-03	3.53E-03	4.50E-06	1.97E-06

At the highest volumetric liquid flux of 0.02357 $m^3.m^{-2}.s^{-1}$, the rate constant for zinc is 1.87 times higher than at the lowest volumetric liquid flux of 0.00471 $m^3.m^{-2}.s^{-1}$. For nickel, the *k* is 1.61 times higher at the highest volumetric liquid flux than at the lowest volumetric liquid flux. Likewise, at the highest volumetric liquid flux, the mass transfer coefficient for zinc is almost 2 times higher than at the lowest volumetric liquid flux, whereas for nickel, the mass transfer coefficient at the highest volumetric liquid flux is approximately 1.6 times higher than at the lowest volumetric liquid flux.

Figure 4.10: Effect of volumetric liquid flux on mass transfer coefficients for Zn^{++} and Ni^{++} during electrochemical treatment using porous corrugated aluminum cathode and SS anode at an applied voltage of 10 V (T = 25°C; pH = 5.6-6; I = 0.155A)

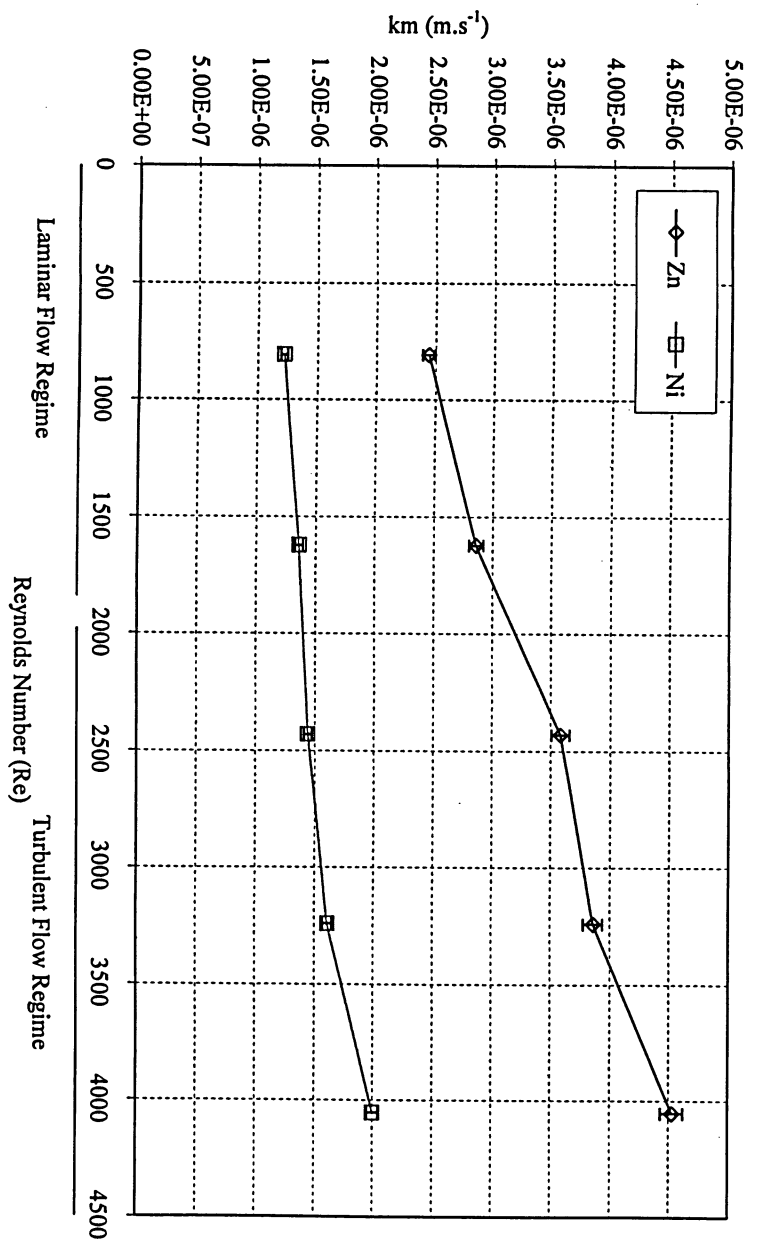

Operating at 10 V, with a volumetric flux of 0.0229 $m^3.m^{-2}.s^{-1}$ in the turbulent region, Mitzakov [15] reported apparent rate constant values of 1.02×10^{-5} s^{-1} for Zn^{++}, and 5.83×10^{-6} s^{-1} for Ni^{++} reduction; after 48 hours of electrochemical treatment, the corresponding rate of reaction (r)values for Zn^{++} and Ni^{++} were 1.97×10^{-8} and 1.5×10^{-8} $kg.m^{-2}.s^{-1}$, respectively (See Appendix A for sample rate of reaction calculations) In the present study, operating under similar conditions (10 V; 0.02357 $m^3.m^{-2}.s^{-1}$), the respective rate constant values for Zn^{++} and Ni^{++} removal are 8.68×10^{-3} and 3.53×10^{-3} $s^{-0.5}$; and for 48 hours of electrochemical treatment, the corresponding rate of reaction values for Zn^{++} and Ni^{++} are 2.64×10^{-8} and 2.11×10^{-8} $kg.m^{-2}.s^{-1}$, respectively, which are approximately 1.4 times higher than those reported by Mitzakov [15].

Similarly, operating at 10 V in the turbulent regime (0.0229 $m^3.m^{-2}.s^{-1}$), the mass transfer coefficients reported by Mitzakov [15] for Zn^{++} and Ni^{++} were 2.05×10^{-6} and 1.19×10^{-6} $m.s^{-1}$, respectively; the values of mass transfer coefficients for Zn^{++} and Ni^{++} obtained in the present study are, respectively, 2.2 and 1.7 times higher than those reported by Mitzakov [15]. Although the amount of supporting electrolyte (500 ppm), the initial concentrations of Ni^{++} and Zn^{++} (20 ppm each), and the volume of simulated wastewater (35 liters) used were same in both studies, the high reaction rates and mass transfer coefficients obtained in the present study may be attributed to the improved configuration of the cathode. In his study, Mitzakov [15] used a plate-in-tank configuration for porous electrodes. In the current study, a flow-through configuration was used, which improved overall kinetics of the process. Moreover, investigations found in the literature reveal that corrugations create irregular flow paths, which help enhance flux and mass transfer rates, and provide characteristics of turbulent regime even at low Reynolds numbers [64]. Therefore, improved mass transfer characteristics exhibited by corrugated structure, could be another reason for the high rate constants and mass transfer coefficients obtained in the present study.

4.3. Observed Deposits on the Cathode

The deposition of Zn^{++} and Ni^{++} on the surface of the corrugated cathode plates was visually observed after 48 hours of treatment. Most of the deposits were formed on the top plate of the stack of corrugated cathodes that directly faced the anode; roughly, 60% of the deposits were found on the top plate. Moving down the stack, the deposition of metal ions gradually decreased on successive plates; the last plate on the bottom had minimal deposition (roughly 5 %). As no technique was employed to measure the amount of metal deposition, the figures provided in the preceding lines are just rough visual estimates.

The deposition trend followed the same path both for laminar and turbulent flows. However, greater product build-up was found in case of turbulent flow. In all cases, the deposits were firm, largely light grey in color, with sparsely distributed dark grey patches. In addition, the perforations on the plates remained unblocked.

Considering the removal trends for Zn^{++} and Ni^{++} presented by Figures 4.1 & 4.3, and the aforementioned observations for metal ions deposits, it may be surmised that during the first 8 hours of electrochemical treatment, the deposition of metal ions mostly occurred on the top cathode plate. Moreover, with the passage of the electrolysis time, the sites for metal ions deposition on the top plate decreased, and they started depositing on the bottom plates.

4.4. Comparison of Porous Corrugated Aluminum Cathode with Porous Aluminum Foam Cathode

As already mentioned in section 3.1.1., a porous aluminum foam cathode was originally used in a flow-through configuration. However, only three runs could be completed using the porous aluminum foam cathode, after which it got degraded and started to chip off.

Figure 4.11 presents a comparison between the porous corrugated aluminum cathode (PCAC) and the porous aluminum foam cathode (PAFC) used in the present study. For the first two runs conducted at an applied voltage of 10 V, and at volumetric fluxes of 0.00471 and 0.00943 $m^3.m^{-2}.s^{-1}$, there was not much difference with respect to the removal of Ni^{++} and Zn^{++} (roughly 5 %) between the two cathodes. However, at a volumetric flux of 0.01414 $m^3.m^{-2}.s^{-1}$, the aluminum foam cathode started to disintegrate. In case of porous aluminum cathode (Figure 4.11), after about 28 hours of electrolysis time, the downward progress of the removal lines for Zn^{++} and Ni^{++} represents degradation phenomenon, after which the loosely deposited Ni^{++} and Zn^{++} started to dissolve again in the bulk solution.

The main reason for degradation of aluminum foam was its brittle structure that could not withstand higher liquid flow rates. Therefore, it may be said that the aluminum foam cathode, if used in flow-through configuration, is not a viable option for removal of Ni^{++} and Zn^{++} from wastewater. In contrast, the porous corrugated aluminum cathode proved to be a stronger electrode that could be used at higher voltages and liquid flow rates. It was used in all subsequent experiments.

Figure 4.11: Comparison between Porous Corrugated Aluminum Cathode and Porous Aluminum Foam Cathode: at different volumetric liquid fluxes and an applied voltage of 10 V (T = 25°C; pH = 5.6-6)

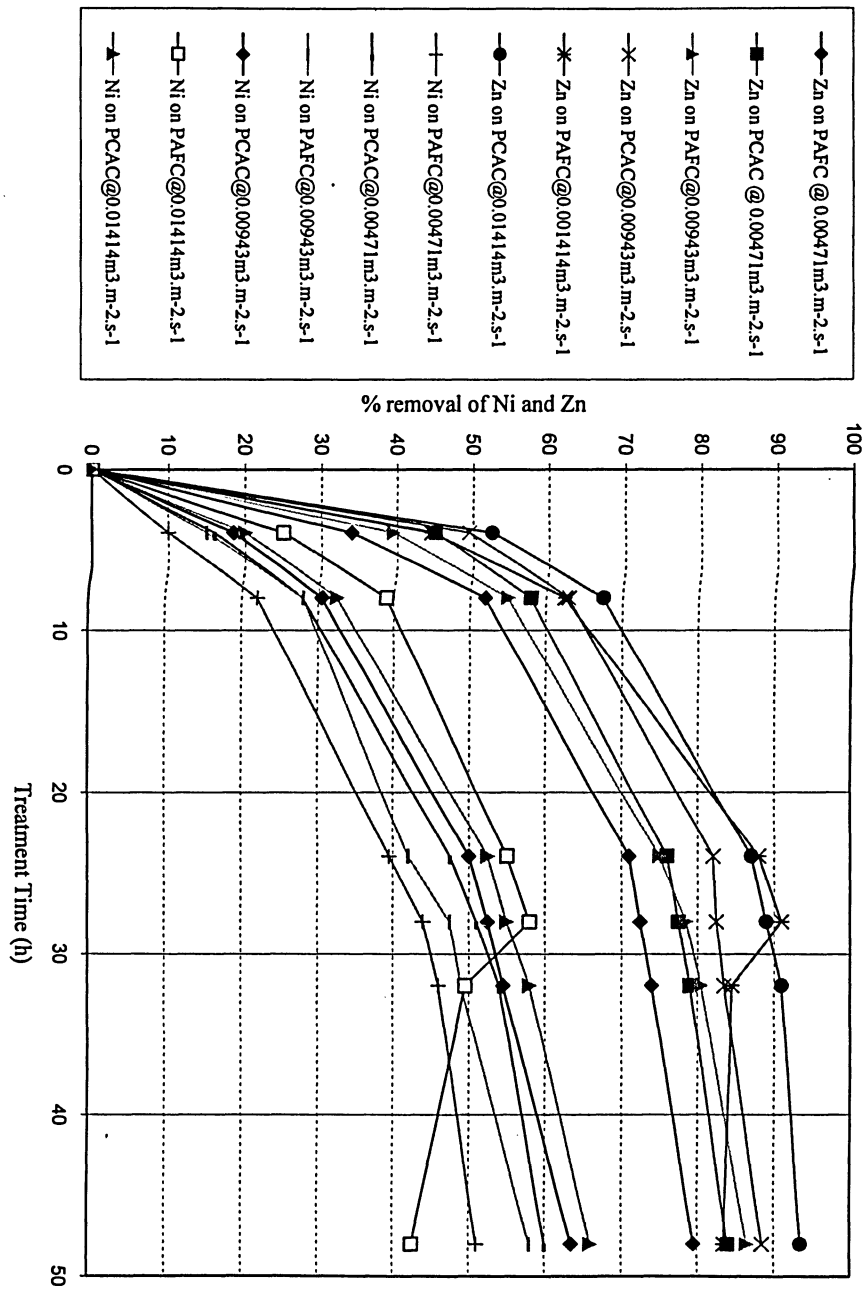

4.5. Optimum Voltage and Volumetric Liquid Flux

From the discussion in the previous sections, it may be concluded so far that the maximum concurrent removal of Zn^{++} and Ni^{++} -- 97 % and 77.5 %, respectively -- occurred at an applied voltage of 10 V, and at a volumetric liquid flux of 0.02357 $m^3.m^{-2}.s^{-1}$(Figure 4.12). This was the maximum volumetric flux that could be achieved under the current system configuration. However, one area that deserved further investigation was the removal of Ni^{++} between applied voltages of 10 and 15 V.

To investigate whether Ni^{++} removal could further be improved, another run was conducted at 12 V and 0.02357 $m^3.m^{-2}.s^{-1}$. Figure 4.13 shows a comparison for percent removal of Zn^{++} and Ni^{++} at 10 and 12 V; it can be observed that operating at 12 V, the removal of Zn^{++} increased only 1 % , while that of Ni^{++} increased 8 %.

Figure 4.14 proves again the square-root relationship of metal ions concentration with time; at an applied voltage of 12 V and at a volumetric liquid flux of 0.02357 $m^3.m^{-2}.s^{-1}$, apparent rate constants for both Zn^{++} and Ni^{++} were obtained from the slopes of the corresponding regression lines. Table 4.4 shows a comparison of rate constants and mass transfer coefficients for Zn^{++} and Ni^{++} at 10 and 12 V and at a volumetric flux of 0.02357 $m^3.m^{-2}.s^{-1}$. A considerable difference was observed in case of nickel removal; for instance, increasing applied voltage from 10 to 12 V, the mass transfer coefficient for Zn^{++} increased by 8 % only, while for Ni^{++} it increased by 27 %.

Table 4.4: Comparison between apparent rate constants and mass transfer coefficients for Zn^{++} and Ni^{++} at 10 and 12 V, and at a constant volumetric flux of 0.02357 $m^3.m^{-2}.s^{-1}$. (T = 25°C; pH = 5.6-6.0)

Applied voltage (V)	Apparent rate constant ($s^{-0.5}$)		Mass transfer co-efficient ($m.s^{-1}$)	
	Zn^{++}	Ni^{++}	Zn^{++}	Ni^{++}
10	8.68E-03	3.53E-03	4.50E-06	1.97E-06
12	1.00E-03	4.36E-03	4.86E-06	2.50E-06

Figure 4.12: Effect of applied voltage on removal of Zn^{++} and Ni^{++} after 48 hours of electrochemical treatment using porous corrugated aluminum cathode and SS anode at volumetric liquid flux of 0.02357 $m^3.m^{-2}.s^{-1}$ (T = 25°C; pH = 5.6-6; I = 0.044, 0.155, 0.260, 0.360 and 0.470 A at applied voltages of 5, 10 ,15 ,20 and 25V, respectively)

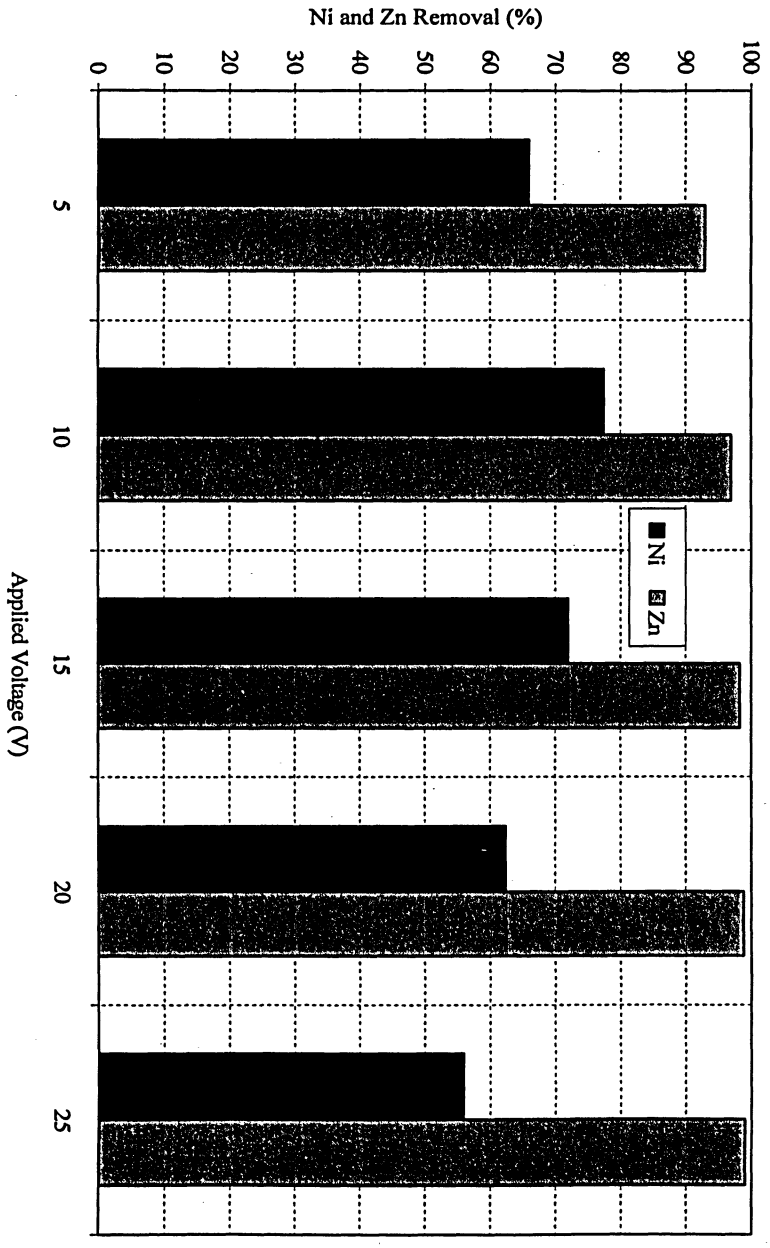

Figure 4.13: Comparison of Zn^{++} and Ni^{++} removal at 10 and 12 V during electrochemical treatment using porous corrugated aluminum cathode and SS anode at volumetric liquid flux of 0.02357 $m^3.m^{-2}.s^{-1}$ (T = 25°C; pH = 5.6-6; I = 0.155 and 0.195 A at applied voltages of 10 and 12 V, respectively)

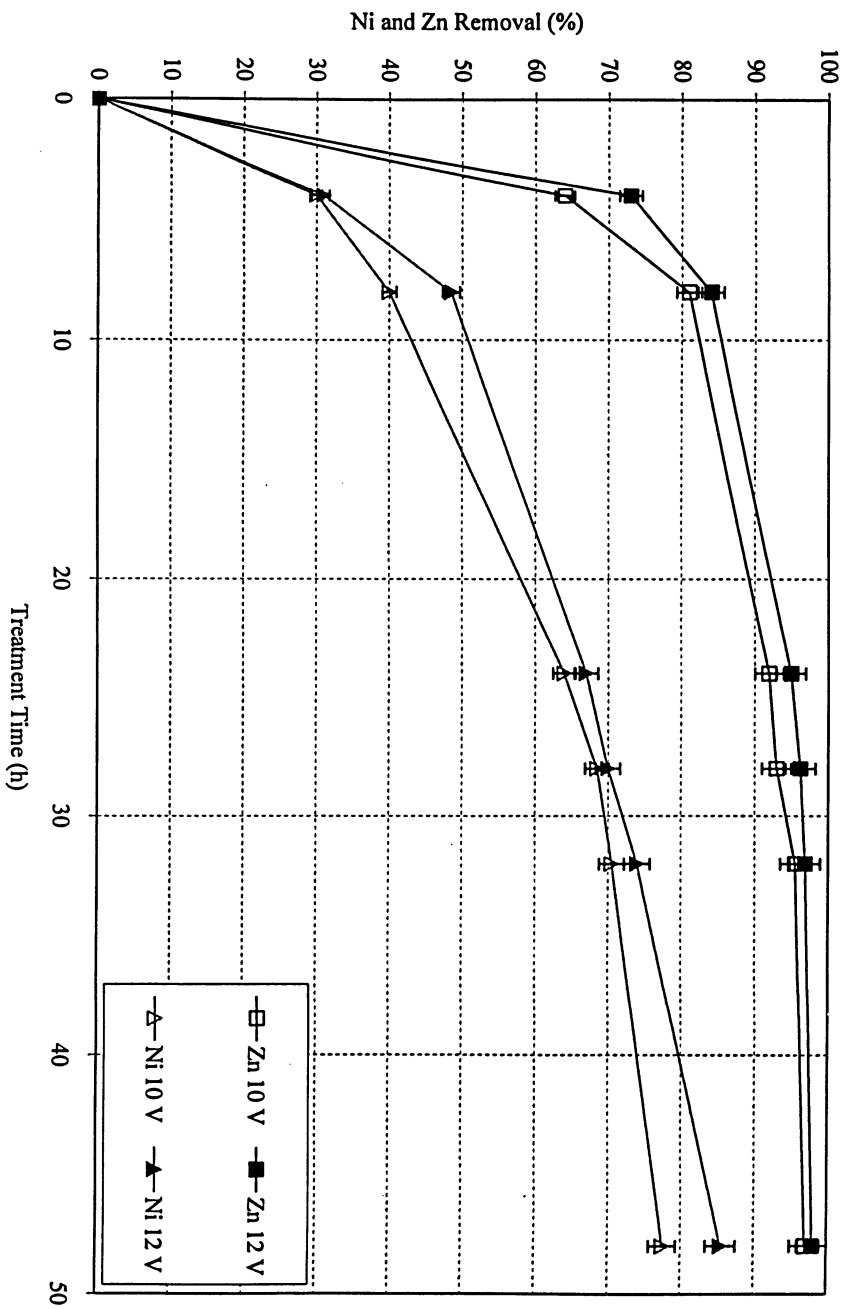

Figure 4.14: Linear regression for Zn^{++} and Ni^{++}: Effect of an applied voltage of 12 V during electrochemical treatment using porous corrugated aluminum cathode and SS anode at volumetric liquid flux of 0.02357 $m^3.m^{-2}.s^{-1}$ (T = 25°C; pH = 5.6-6; I = 0.195 A). Solid line is linear regression

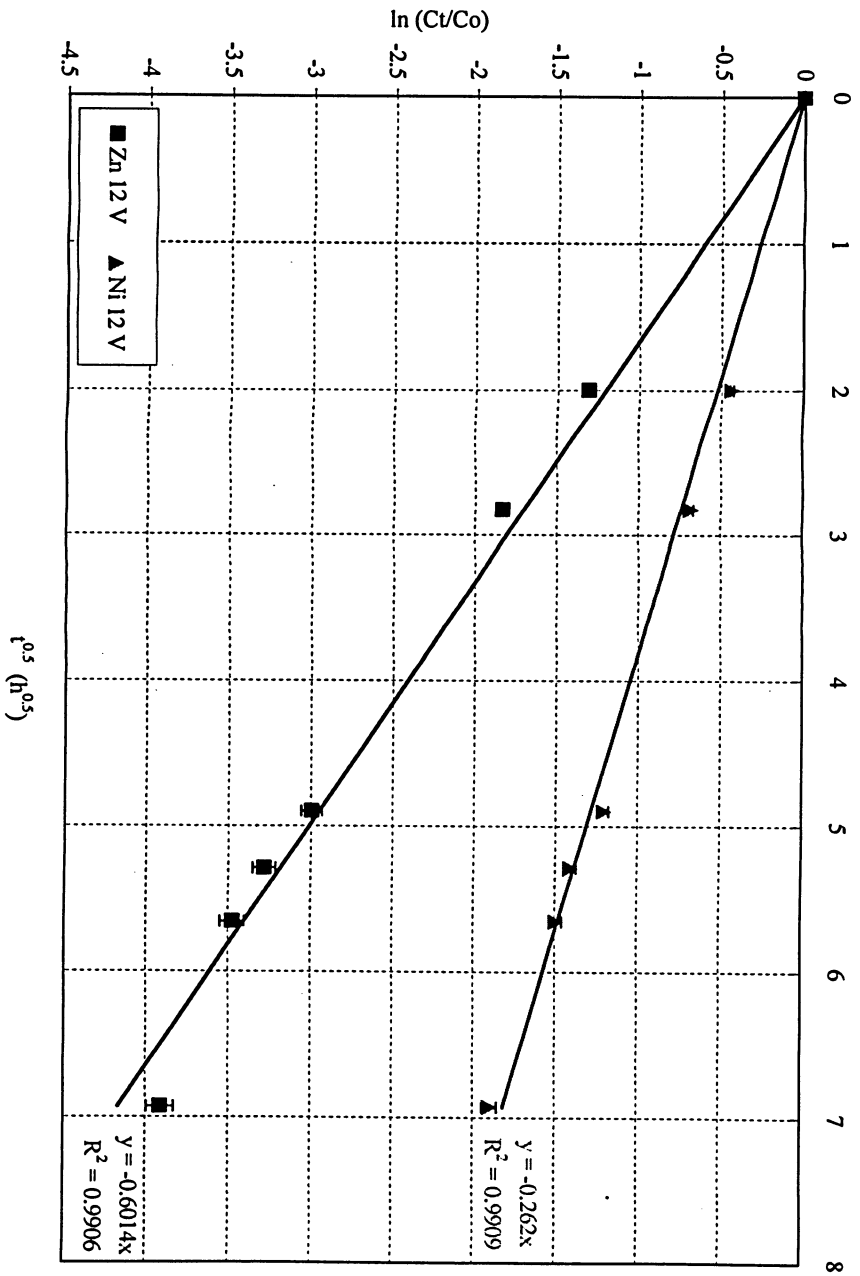

At an applied voltage of 12 V, a small amount of precipitation for nickel (0.37 $mg.l^{-1}$) was observed at the end of 48 hours of treatment. Operating beyond 12 V would have resulted in increased precipitation for Ni^{++}, as was observed in case of an applied voltage of 15 V. Therefore, for the present study, the optimum applied voltage and volumetric liquid flux were found to be 12 V and 0.02357 $m^3.m^{-2}.s^{-1}$, respectively.

The run at the optimum applied voltage and volumetric liquid flux was repeated three times. The standard deviations for measurement of Zn^{++} and Ni^{++} concentration were found to be 0.063 and 0.071$mg.l^{-1}$, respectively. Likewise, the percentage errors associated with the measurements of zinc and nickel ions concentration were found to be 2.1% and 2.4%, respectively; these errors were assumed to be same for all other runs.

5. Conclusions

The present study investigated the electrochemical removal of nickel and zinc ions from simulated wastewater using porous electrodes in a flow-through configuration. From the analysis of the results obtained, the following conclusions could be drawn:

- The applied voltage had a definite effect on the removal of nickel and zinc; the maximum concurrent removal for both nickel and zinc occurred at an applied voltage of 12 V. Although the removal of Zn^{++} increased with the increase in the applied voltage, it only improved by 1 %, from 98% to 99.05 %, when the voltage was increased from 12 to 25 V; nevertheless, the effect of applied voltage was more pronounced in case of nickel; the removal of nickel ions decreased from a value of 85.5 % at 12 V to 56 % at 25 V.
- Increasing volumetric liquid flux from laminar to turbulent conditions significantly improved the removal of both nickel and zinc ions; operating at an applied voltage of 10 V and a volumetric liquid flux of 0.02357 $m^3.m^{-2}.s^{-1}$ in the turbulent regime, the removal for nickel and zinc ions increased by 17.5 % and 13 %, respectively, when compared to their corresponding removal at a volumetric liquid flux of 0.00471 $m^3.m^{-2}.s^{-1}$ in the laminar regime.
- Using a stack of porous corrugated aluminum plates as cathode, and porous stainless steel as anode in a flow-through configuration proved to be a viable option for the removal of nickel and zinc ions from the simulated wastewater.

6. Recommendations

The present study showed that Ni^{++} and Zn^{++} could be removed from simulated wastewater using flow-through porous electrodes. The separation between the anode and the cathode is of prime importance with respect to electrochemical reactor design. If the distance between the anode and the cathode is decreased, the resistance to flow of the current decreases as well. Therefore, further study should be conducted to investigate the effect of separation between the anode and the cathode on the removal of heavy metals from wastewater Moreover, the porous corrugated electrodes could be used in an alternating flow-through arrangement; this may result in improved current densities even at lower applied voltages. Furthermore, the removal of individual metals, such as zinc and nickel should also be studied to determine the influence of one metal on the electrodeposition of the other.

References

1. Koene, L. and L.J.J. Janssen, *Removal of Nickel from Industrial Process Liquids,* Electrochimica Acta, **47** 695-703 (2001).
2. Kanluen, R. and S.I. Amer, *Treating Plating Wastewater*, www.pfonline.com Date accessed: (17/04/2005).
3. Zaki, N. *Corrosion Potential of Zinc Alloys*, www.pfonline.com/articles/039902 Date accessed: (17/04/2005).
4. Lancaster, R. and M. Rizzone, *Ultrafiltration Removes Metals from Wastewater*, Toyota Manufacturing Kentucky, Georgetown, Kentucky. (http://www.pfonline.com/articles/00sum04.html) Date accessed: (20/04/2005).
5. Doan, H.D., J. Wu, E. Boithi and M. Storrar, *Treatment of Wastewater using a Combined Biological and Electrochemical Technique*, Journal of Chemical Technology and Biotechnology, **78** 632-641 (2004).
6. United States Environmental Protection Agency, *Development Document for the Final Effluent Limitations: Guidelines and Standards for the Metal Products and Machinery Point Source Category*, US EPA Washington D.C., 2003. (http://www.epa.gov/waterscience/guide/mpm/tdd.htm) Date accessed: (2005).
7. Chapter 681, Sewers, Article 1, *Sewage and Land Drainage, By-Law No. 457-2000*, Toronto Municipal Code Sewers, City of Toronto, Ontario, Canada (http://www.city.toronto.on.ca/legdocs/bylaws/2000/law0457.pdf) Date accessed: (2005).
8. Weininger, J.L. in: *Tutorial Lectures in Electrochemical Engineering and Technology* (R. Alkire and T. Beck eds.), AIChE Symposium Series 204, **77** 180 (1981).
9. Carlo, S. M. Panizza, P. Paganelli and Giacomo Cerisola, *Electrochemical Remediation of Copper (II) from an Industrial Effluent Part 1: Monopolar Plate Electrodes*, Resources Conservation and Recycling, **26** 115-124 (1999).
10. Juttner, K., U. Galla and H. Schmieder, *Electrochemical Approaches to Environmental Problems in the Process Industry*, Electrochimica Acta, **45** 2575-2594 (2000).

11. Guohua, C., *Electrochemical Technologies in Wastewater Treatment*, Separation and Purification Technology, **38** 11-41 (2004).

12. Veglio F., R. Quarisam, P. Fornari and S. Ubaldini, *Recovery of Valuable Metals from Electronic and Galvanic Industrial Wastes by Leaching and Electrowinning*, Waste Management, **23** 245-252 (2003).

13. Muresan L., G. Maurin, L. Oniciu and S. Avram, *Effects of Additives on Zinc Electrowinning from Industrial Waste Products*, Hydrometallurgy, **40** 335-342 (1996).

14. Sider M., C. Fan and D.L. Piron, *Effects of Copper and Anions on Zinc-Nickel Anomalous Codeposition in Plating and Electrowinning*, Journal of Applied Electrochemistry, **31** 313-317 (2001).

15. Mitzakov R, *Combined Electrochemical & Biological Treatment of Industrial Wastewater using Porous Electrodes and a Packed Bed Reactor*, M.A.Sc. Thesis, Department of Chemical Engineering, Ryerson University, Toronto, Ontario, Canada (2004).

16. Christopher, M. A. B. and A.M.O. Brett, *Electrochemistry Principles, Methods and Applications*, 4th ed., Oxford University Press Inc., New York, (1998).

17. Goodridge, F. and K. Scott, *Electrochemical Process Engineering: A Guide to the Design of Electrolytic Plant*, Plenum Press, New York, (1995).

18. Pletcher, D. and F. Walsh, *Industrial Electrochemistry*, 2nd ed., Chapman-Hall, London, (1990).

19. Prentice, G., *Electrochemical Engineering Principles*, Prentice-Hall Inc., New Jersey, (1991).

20. Oldham, K. and J. Myland, *Fundamentals of Electrochemical Science*, Academic Press, San Diego, CA, (1994).

21. Vaaler, L.E. in: *Tutorial Lectures in Electrochemical Engineering and Technology* (R. Alkire and T. Beck eds.), AIChE Symposium Series 204, **77** 171-177 (1981).

22. Abda, M., Z. Gavra and Y. Oren, *Removal of Chromium from Aqueous Solutions by Treatment with Fibrous Carbon Electrodes: Column Effects*, Journal of Applied Electrochemistry, **21** 734-739 (1991).

23. Carta, R., S. Palmas, A.M. Polcaro, G. Tola, *Behaviour of a Carbon Felt Flow-by Electrode Part 1: Mass Transfer Characteristics*, Journal of Applied Electrochemistry, **21** 793-798 (1991).
24. Delanghe, B., S. Tellier and M. Astruc, *Mass Transfer to a Carbon or Graphite Felt Electrode*, Electrochimica Acta, **35** 1369-1376 (1990).
25. Kinoshita, K. and S.C. Leach, *Mass Transfer Study of Carbon Felt Flow-through Electrode*, Journal of Electrochemical Society **129** 1993-1997 (1982).
26. Vatistas, N., P.F. Marconi and M. Bartolozzi, *Mass Transfer Study of the Carbon Felt Electrode*, Electrochimica Acta, **36** 339-343 (1991).
27. Marracino, J.M., F. Coeuret and S. Langlois, *A First Investigation of Flow-through Porous Electrodes Made of Metallic Felts or Foams*, Electrochimica Acta, **32** 1303-1309 (1987).
28. Grau, J.M and J.M. Bisang, *Removal and Recovery of Mercury from Chloride Solutions by Contact Deposition on Iron Felt*, Journal of Chemical Technology and Biotechnology, **62** 153-158 (1995).
29. Lizarraga, D.S. and J.M. Bisang, *Mass Transfer at Iron Felts*, Journal of Applied Electrochemistry, **25** 1209-1215 (1996).
30. Leroux, F. and F. Coeuret, *Flow-by Electrodes of Ordered Sheets of Expanded Metal 1: Mass Transfer and Current Distribution*, Electrochimica Acta, **30** 159-165 (1985).
31. Sioda, R.E., *Mass Transfer Problems in Electrolysis with Flowing Solution on Single and Stacked Screens*, Journal of Electroanalytical Chemistry, **70** 49-54 (1976).
32. Storck, A., P.M. Robertson and N. Ibi, *Mass Transfer Study of Three-dimensional Electrodes Composed of Stacks of Nets*, Electrochimica Acta, **24** 373-380 (1979).
33. Schmal, D.J., V. Erkel and P.J. Van Duin, *Mass Transfer at Carbon Fiber Electrodes*, Journal of Applied Electrochemistry, **16** 422-430 (1986).
34. Enriquez-Granados, D. Hutin and A. Strock, *The Behaviour of Porous Electrodes in a Flow-by Regime II: Experimental Study*, Electrochimica Acta, **27** 303-311 (1982).

35. Simonsson, D., *A Flow-by Packed Bed Electrode for Removal of Metal Ions from Waste Waters*, Journal of Applied Electrochemistry, **14** 595-604 (1984).

36. Higashi, K., H. Fukushima, T. Urakawa, T. Adaniya and K. Matsudo, *Mechanism of Zinc Alloys Containing a Small Amount of Cobalt*, Journal of Electrochemical Society, **128** 2081-2085 (1981).

37. Lanza, M.R.V. and R. Bertazzoli, *Removal of Zinc (II) from Chloride Medium using a Porous Electrode: Current Penetration within the Cathode*, Journal of Applied Electrochemistry, **30** 61-70 (2000).

38. Pletcher, D., I. Whyte, F.C. Walsh and J.P. Millington, *Reticulated Vitreous Carbon Cathodes for Metal Ion Removal from Process Streams Part I: Mass Transport Studies*, Journal of Applied Electrochemistry, **21** 659-666 (1991).

39. Podlaha, E.J. and J.M. Fenton, *Characterization of a Flow-by RVC Electrode Reactor for the Removal of Heavy Metals from Dilute Solutions*, Journal of Applied Electrochemistry, **25** 229-306 (1995).

40. Ponce de Leon, C. and D. Pletcher, *The Removal of Pb (II) from Aqueous Solutions using a Reticulated Vitreous Carbon Cathode Cell: Influence of the Electrolyte Medium*, Electrochimica Acta, **41** 533-540 (1996).

41. Wang, J. and H.D. Dewald, *Deposition of Metals at a Flow-through Reticulated Vitreous Carbon Electrode Coupled with On-line Monitoring of the Effluent*, Journal of Electrochemical Society, **139** 1814-1818 (1983).

42. Langlois, S. and F. Coeuret, *Flow-through and Flow-by Porous Electrodes of Nickel Foam. Part II: Diffusion-convective Mass Transfer between Electrolyte and Foam*, Journal of Applied Electrochemistry, **19** 51-60 (1989).

43. Langlois, S. and F. Coeuret, *Flow-through and Flow-by Porous Electrodes of Nickel Foam. Part I: Material Characterization*, Journal of Applied Electrochemistry, **19** 43-50 (1989).

44. Montillet, A., J. Comiti and J. Legrand, *Application of Metallic Foams in Electrochemical Reactors of the Filter-press Type, Part II: Mass Transfer Performance*, Journal of Applied Electrochemistry, **24** 384-389 (1994).

45. Panizza, M., C. Solisio and C. Giacomo, *Electrochemical Remediation of Copper (II) from an Industrial Effluent Part II: Three-dimensional Foam Electrodes*, Resources Conservation and Recycling, **27** 299-307 (1999).

46. Tentorio, A. and U. Casolo-Ginelli, *Characterization of Reticulate, Three-dimensional Electrodes*, Journal of Applied Electrochemistry, **8** 195-205 (1978).

47. Bennion, D.N. and J. Newman, *Electrochemical Removal of Copper Ions from very Dilute Solutions*, Journal of Applied Electrochemistry, **2** 113-122 (1972).

48. Al-Shammari, A.A., S.U. Rahman and D.T. Chin, *An Oblique Rotating Barrel Electrochemical Reactor for Removal of Copper Ions from Wastewater*, Journal of Applied Electrochemistry, **34** 447-453 (2004).

49. Kim, Y.U., H.W. Cho, H.S. Lee, C.K. Lee, J.C. Lee, K.I. Rhee, H.J.,Sohn and T. Kang, *Electrowinning of Palladium using a Modified Cyclone Reactor*, Journal of Applied Electrochemistry, **32** 1235-1239, (2002).

50. Winder, R.C., M.F. Sousa and R. Bertazzoli, *Electrolytic Removal of Lead using a Flow-through Cell with a Reticulated Vitreous Carbon Cathode*, Journal of Applied Electrochemistry, **25** 201-207 (1998).

51. Njau, K.N., M. V. Woude, G.J. Visser and L.J.J. Janssen, *Electrochemical Reduction of Nickel Ions from Dilute Artificial Solutions in a GBC Reactor*, Journal of Applied Electrochemistry, **28** 689-696 (1998).

52. Orhan, G., C. Aslan, H. Bombach and M. Stelter, *Nickel Recovery from the Rinse Waters of Plating Baths*, Hydrometallurgy, **65** 1-8 (2002).

53. Taylor, J.R. *An Introduction to Error Analysis*, 2nd edition, University Science Books, Sausalito, California (1997).

54. Kline, S.J and F.A. McClintock, *Describing Uncertainties in Single Sample Experiments*, Mechanical Engineering, **75** 3-8, January (1953).

55. Crank, J., *The Mathematics of Diffusion*, 2nd edition, Oxford University Press, London, (1975).

56. Brenner, A. *Electrodeposition of Alloys: Principles and Practice*, Vol. 1&2, Academic Press, New York (1963).

57. Dahms, H. and M. Croll, *The Anomalous Codeposition of Iron-Nickel Alloys*, Journal of Electrochemical Society, **112** 771-775 (1965).

58. Fukushima, H., T. Akiyama, K. Higashi, R. Kammel, and M. Karimkhani, *Removal of Zinc, Cobalt and Nickel from Wastewater*, METALL, **42** 242-250 (1988).

59. Fabri Miranda, F.J., O.E. Barcia, O.R. Mattos and R. Wiart, *Electrodeposition of Zn-Ni Alloys in Sulfate Electrolytes 1. Experimental Approach*, Journal of Electrochemical Society, **144** 3441-3448 (1997).

60. Chassaing, E. and R. Wiart, *Electrocrystallization Mechanism of Zn-Ni Alloys in Chloride Electrolytes*, Electrochimica Acta, **37** 545-553 (1992).

61. Ishihara, M., H. Yumoto, K. Akashi and K. Kamei, *Zinc-Nickel Alloy Whiskers Electrodeposited from a Sulfate Bath*, Materials Science and Engineering, **B 38** 150-155 (1996).

62. Atkins, P. and L. Jones, *Chemistry: Molecules, Matter and Change*, 3rd ed., W.H. Freeman and Company, New York (1997).

63. Private communications with Dr. Huu D. Doan, Department of Chemical Engineering, Ryerson University, Toronto, Ontario, Canada (2005).

64. Tzanetakis, N., K. Scott, W.M. Taama and R.J.J. Jachuck, *Mass Transfer Characteristics of Corrugated Surfaces*, Applied Thermal Engineering, **24** 1865-1875 (2004).

65. Aseyev, G.G., *Electrolytes Transport Phenomenon: Methods for Calculation of Multicomponent Solutions and Experimental Data on Viscosities and Diffusion Coefficients*, Begell House, New York (1998).

66. Green D.W. and J.O. Maloney, *Perry's Chemical Engineers Handbook*, 7th edition. McGraw Hill, New York (1997).

Appendices

Appendix A: Sample Calculations

Appendix A1: Orifice Diameter Calculation

To determine orifice diameter, first the liquid velocity was calculated using the following equation [63]:

$$\Delta P = 1.7267 \times 10^{-4} \rho v^2 \qquad \text{(A1-1)}$$

In the above expression, ΔP is the differential pressure in lb.ft^{-2}, ρ is the density of the liquid in lb ft^{-3}, and v is the liquid velocity in ft.s^{-1}. The pressure difference is the pressure exerted by the column of water at the base of the electro-cell. In the design of the electrochemical cell, the height of the liquid head was chosen to be 30.48 cm or 1ft.

Density of water at 25°C, $\rho = 62.24\, lb.ft^{-3}$

At one foot liquid head, $\Delta P = 62.42\, lb.ft^{-2}$

$$v = \sqrt{\frac{62.42}{62.24(1.7267 \times 10^{-4})}} = 76.21\, ft.s^{-1}$$

For a liquid flow rate (Q) of 25 l.min^{-1} = 0.01471 ft^3.s^{-1}, which was the maximum flow rate of wastewater in the experimental design for current study (see Appendix A4), the orifice diameter was calculated from the following equation:

$$D_{orifice} = \sqrt{\frac{4Q}{\pi v}} \qquad \text{(A1-2)}$$

$$D_{orifice} = \sqrt{\frac{4Q}{\pi v}} = \sqrt{\frac{4 \times 0.01471}{\pi \times 76.21}} = 0.016\, ft = 0.00487 m \cong 0.5\, cm$$

At the highest volumetric liquid flux of 0.02357 m^3.m^{-2}.s^{-1}, with all the orifices left open (see fig 3.2 d), the volumetric flux through a single orifice was 0.00295 m^3.m^{-2}.s^{-1}

Appendix A2: Calculation of Surface Area of the Anode [63]

The porous anode was constructed by compressing 316-stainless steel netting in between two 316-stainless steel meshes. In one layer of netting, there were approximately 40 wires of an approximate length of 16.5 cm. The diameter of one wire was 0.016 cm. The dimensions of one layer of was 11.4 × 10.8 cm. Based on these values the porosity of the anode was calculated.

Volume of one layer (solid) $= (11.4 \times 10.8 \times 0.016) cm^3 = 1.974 cm^3$

Volume of one wire $= \frac{\pi D^2 L}{4} = \frac{\pi (0.016 cm)^2 16.5 cm}{4} = 0.00332 cm^3$

Volume of 40 wires in a layer $= 40 \times 0.00332 cm^3 = 0.133 cm^3$

The porosity of the anode $(\varepsilon) = 1 - \left(\frac{0.133 cm^3}{1.974 cm^3} \right) = 0.933$

r = ratio of surface area to volume of the wire $= \frac{4}{D} = \frac{4}{0.016} = 250\ cm^{-1}$

The resulting specific area of the anode is [31]:

Specific area of the anode $= r.(1-\varepsilon) = 250\ cm^{-1}(1-0.933) = 16.75\ cm^{-1}$

Appendix A3: Viscosity and Density Calculations [65]

The dynamic viscosity of the simulated wastewater was calculated from the method described in [65].The dynamic viscosity (η) of a multicomponent electrolytic solution can be calculated from the following expression:

$$\eta = \eta_o \exp V \qquad \text{(A3-1)}$$

In the above expression η_o is the viscosity of water, which was obtained from Perry's Chemical Engineers' Handbook [66] at the experimental temperature. V was given by the following equation:

$$V = \sum_{i=1}^{k} c_i (A_{0i} + A_{1i}t + A_{2i}c_i + A_{3i}t) \qquad \text{(A3-2)}$$

In the above expression, c_i is the percent mass fraction of species i, A_{ij} are coefficients for each electrolyte. The reported percent error of these coefficients for zinc sulfate, nickel sulfate and potassium sulfate was 2.39 %, 1.54 %, and 0.30 %, respectively.

To determine the mass fraction of each species the density of the solution was required. The density of the solution was calculated from the following formula:

$$\rho = \rho_o + \sum_{i=1}^{k} c_i (B_{1i} + B_{2i}t + B_{3i}c_i) \qquad \text{(A3-3)}$$

In the above expression ρ_o is the density of water (kg.m^{-3}), B_{ij} are the coefficients for the electrolytic species present. The reported error for these coefficients for zinc sulfate, nickel sulfate and potassium sulfate was 0.27%, 0.23% and 0.13%, respectively. The density of the water was obtained from Perry's Chemical Engineers Handbook [66] at the experimental temperature of 25°C.

The density expression required the % mass fraction of each species. An iterative process was required of this. Therefore, the following expression was used with an initial value of the density of the solution selected:

$$c_i = \frac{100 M_i C_i}{\rho} \qquad \text{(A3-4)}$$

In the above expression, c_i is the mass fraction of species, M_i is the molecular weight of the species, and C_i is the mass concentration of the species. The mass fraction of each species was determined when a prescribed tolerance was reached. With the mass fraction calculated, the dynamic viscosity of the solution was calculated from equation (A3-1).

The density and dynamic viscosity calculated for a multicomponent electrolytic solution with concentration of 20 ppm for zinc and nickel, and 500 ppm for potassium sulfate were:

- $\rho = 997.31\ g.l^{-1} = 997.31\ kg.m^{-3}$
- $\eta = 0.00087\ Pa.s = 0.00087.kg.m^{-1}.s^{-1}$

Appendix A4: Calculation of Volumetric Liquid Flux and Reynolds Number

The Reynolds number is the ratio of inertial forces, as described by Newton's second law of motion, to viscous forces. If the Reynolds number is high, inertial forces dominate and turbulent flow exists. If it is low, viscous forces prevail, and laminar flow results. For a fluid flowing through a pipe or column, the Reynolds number is given by the following expression:

$$Re = \frac{uD_C}{\upsilon} \qquad \text{(A4-1)}$$

In the above expression, u is the characteristic velocity of the fluid ($m.s^{-1}$), D_C (m) is the characteristic diameter of the column, and υ is the kinematic viscosity of the fluid. The characteristic velocity of a fluid flowing through a pipe depends on pipe diameter. If the diameter of the pipe varies, the velocity of the fluid varies as well. However, if the pipe is of uniform diameter, as was the case in the present study, the characteristic velocity is equal to the volumetric flux of the fluid (U) ($m^3.m^{-2}.s^{-1}$). Likewise, the characteristic diameter depends on the particular geometry of the pipe, and in case of a uniform diameter pipe, it is equal to the actual diameter of the pipe. In the present study, the PVC column had a uniform diameter, therefore, D_C was equal to the diameter of the electrochemical cell ($D_{Cell} = 0.15m$); and kinematic viscosity ($\upsilon = \eta / \rho$, $m^2.s^{-1}$) was calculated from the values of dynamic viscosity and density given in Appendix A3.

In the present study, the flow rate was varied between 5 $l.min.^{-1}$ to 25 $l.min^{-1}$. The volumetric liquid flux (U) was calculated by dividing the flow rate with area of the

electrochemical cell (A_{Cell}). The calculations for different volumetric liquid fluxes and Reynolds numbers are provided in Table A4-1.

Table A4-1: Volumetric liquid fluxes and Reynolds numbers at different flow rates (D_{Cell} =.0.15m; A_{Cell} = 0.01767 m^2; $\upsilon = 8.72\times10^{-7} m^2.s^{-1}$)

Liquid flow rate (Q)		Volumetric liquid flux ($U = Q/A_{Cell}$)	$Re = \frac{U D_{Cell}}{\upsilon}$
($l.min^{-1}$)	($m^3.s^{-1}$)	($m^3.m^{-2}.s^{-1}$)	
5	8.33E-5	0.00471	810
10	1.66E-4	0.00943	1622
15	2.50E-4	0.01414	2432
20	3.33E-4	0.01886	3244
25	4.16E-4	0.02357	4054

Appendix A5: Rate of Reaction Calculation

In the present study, the following equation of was used to calculate rate of reaction (r) for Zn^{++} and Ni^{++} [63]:

$$r = \frac{V\Delta C}{A\Delta t} \qquad \text{(A5-1)}$$

Where V is the total volume of the electrolyte, ΔC is the change in the concentration of metal ions in the time interval Δt, and A is the area of the cathode

For 48 hours of electrochemical treatment at an applied voltage of 10 V, and at a volumetric liquid flux of 0.02357$m^3.m^{-2}.s^{-1}$ (Fig. 4.6), C_t for zinc can be calculated from eq. (4.1) as follows:

$$\ln\left(\frac{C_t}{C_o}\right) = -kt^{1/2} \text{ or } C_t = C_o \exp\left[-kt^{1/2}\right] = 20\exp\left[-0.521(48)^{1/2}\right] = 0.54\, mg.l^{-1}$$

So, for zinc:

$$\Delta C = C_o - C_t = C_0 - C_{48} = 20 - 0.54 = 19.46(mg.l^{-1}) = 19.46g.m^{-3}$$

$$\Delta t = t_{48} - t_o = 48 - 0 = 48(h)\ ;\ A = 0.1507\text{m}^2;\ V = 0.035\text{m}^3$$

$$r = \frac{0.035(19.46)}{0.1507(48)} = 0.095g.m^{-2}.h^{-1} = \frac{0.095}{1000\times 3600} kg.m^{-2}.s^{-1} = 2.64\times 10^{-8} kg.m^{-2}.s^{-1}$$

Similarly, for nickel $r = 2.11\times 10^{-8} kg.m^{-2}.s^{-1}$

And using the model equation of Mitzakov's work [15], $(\ln(C_t / C_o) = -kt)$, with A=0.1669m^2 and V=0.035 m^3, in his study, the corresponding rate of reaction values for zinc and nickel were found to be 1.97 × 10^{-8} and 1.5 × 10^{-8} kg.m^{-2}.s^{-1}, respectively.

Appendix A6: Calculation of the Mass Transfer Coefficient [63]

The mass transfer coefficients for nickel and zinc were calculated using average metal ions concentration Ć (mg.l^{-1}), and the change in metal ions concentration ΔC (mg.l^{-1}) during the specific time interval Δt (h). One sample calculation for determining k_m for zinc at a volumetric liquid flux of 0.02357 m^3.m^{-2}.s^{-1} and at an applied voltage of 10 V is shown below in Table A6-1:

Table A6-1: Mass transfer coefficient for Zn^{++}

Time (h)	Conc. Zn (mg.l^{-1})	$\Delta t = t_2 - t_1$ (h)	$\Delta C = C_1 - C_2$ (mg.l^{-1})	$\acute{C} = (C_1+C_2)/2$ (mg.l^{-1})	$k_m = V\Delta C/\Delta t.A.\acute{C}$ (m.h^{-1})	$k_m \Delta t$ (m)
0	20	4	12.8	13.6	0.054646942	0.218587767
4	7.2	4	3.4	5.5	0.035893105	0.14357242
8	3.8	16	2.2	2.7	0.011827521	0.189240335
24	1.6	4	0.2	1.5	0.00774165	0.0309666
28	1.4	4	0.5	1.15	0.025244511	0.100978044
32	0.9	16	0.3	0.75	0.005806238	0.092899801
48	0.6				Avg. k_m =	**0.01617**

where V= 0.035 m^3 = volume of the solution and A= 0.1507 m^2 is the area of the cathode, and Avg. $k_m = (\sum k_m \Delta t)/48h = 0.0162 m.h^{-1} = 4.5 \times 10^{-6}$ m.s^{-1}

Appendix A7: Uncertainty in Mass Transfer Coefficient

The mass transfer coefficient was given by the following expression [63]:

$$k_m = \frac{\Delta C V}{\Delta t A e C'} \tag{A7-1}$$

The uncertainties associated with the mass transfer coefficients for zinc and nickel were calculated by the method of Kline and McClintock based on the following error propagation equation [54]:

$$\sigma^2 x \approx \sigma^2 u \left(\frac{\partial x}{\partial u}\right)^2 + \sigma^2 v \left(\frac{\partial x}{\partial v}\right)^2 + ... \tag{A7-2}$$

Based on equation A7-2, the uncertainty associated with the mass transfer coefficient was given by

$$k_m = \sqrt{\left(\frac{\partial km}{\partial \Delta C}\cdot\sigma_{\Delta C}\right)^2 + \left(\frac{\partial km}{\partial V}\cdot\sigma_V\right)^2 + \left(\frac{\partial km}{\partial \Delta t}\cdot\sigma_{\Delta t}\right)^2 + \left(\frac{\partial km}{\partial Ae}\cdot\sigma_{Ae}\right)^2 + \left(\frac{\partial km}{\partial C'}\cdot\sigma_{C'}\right)^2} \tag{A7-3}$$

A sample calculation for determining the uncertainty linked with mass transfer coefficient for zinc (Run 10: at 12 V and 0.02357 $m^3.m^{-2}.s^{-1}$) is provided below.

1. The uncertainty associated with ΔC in time interval Δt was calculated by multiplying the total concentration change in 48 hours by standard deviation for zinc (0.063 $mg.l^{-1}$):

$$\sigma_{\Delta C} = \Delta C \times 0.063 = 19.6 \times 0.063 = 1.23 mg.l^{-1}$$

2. Similarly, the uncertainty for average concentration (C') was:

$$\sigma_{C'} = C' \times 0.063 = 10.2 \times 0.063 = 0.642 mg.l^{-1}$$

3. The uncertainty in total volume of the electrolyte was based on a 4000 Erlenmeyer flask, which was used to make scale markings on the holding tank to a total of 35 liters of solution. The flask had an uncertainty of ± 5% or ± 200 ml. For 35 liters of solution, the total uncertainty was:

$\sigma_V = 8(4000 \pm 200)ml + 3000 \pm 150ml = 35000 \pm 1750ml \cong 35000 \pm 2l$, or $\sigma_V = 0.002m^3$

4. The uncertainty in electrode surface area was based on the graduations of the measuring tape used. The smallest graduation was 1mm. The relative uncertainty associated with electrode area (cathode) was calculated by the following expression [54]:

$$\text{Relative uncertainty} = \sqrt{\left(\frac{0.1}{9}\right)^2 + \left(\frac{0.1}{21}\right)^2} = 1.2\%$$

Or

$$\sigma_{Ae} = 0.012(0.1507)m^2 = 1.81 \times 10^{-3} m^2$$

5. The uncertainty associated with time was based on an assumed error of 5 seconds in an hour, and for 48 hours of electrolysis time it amounted to

$$\sigma_{\Delta t} = 48 \times 5/3600 = 0.067h$$

The uncertainty associated with k_m was determined by calculating the five terms in equation C4-3 one by one

$$\left(\frac{V}{\Delta t.Ae.C'} \times \sigma_{\Delta C}\right)^2 = \left(\frac{0.035}{48 \times 0.1507 \times 10.2} \times 1.23\right)^2 = 3.4 \times 10^{-7} m.h^{-1}$$

$$\left(\frac{\Delta C}{\Delta t.Ae.C'} \times \sigma_V\right)^2 = \left(\frac{19.6}{48 \times 0.1507 \times 10.2} \times 0.002\right)^2 = 2.82 \times 10^{-7} m.h^{-1}$$

$$\left(\frac{\Delta C}{(\Delta t)^2.Ae.C'}\times\sigma_{\Delta t}\right)^2=\left(\frac{19.6\times0.035}{(48)^2\times0.1507\times10.2}\times0.067\right)^2=1.68\times10^{-10}m.h^{-1}$$

$$\left(\frac{\Delta C}{\Delta t.(Ae)^2.C'}\times\sigma_{Ae}\right)^2=\left(\frac{19.6\times0.035}{48\times(0.1507)^2\times(10.2)}\times1.81\times10^{-3}\right)^2=1.24\times10^{-8}m.h^{-1}$$

$$\left(\frac{\Delta C}{\Delta t.Ae.(C')^2}\times\sigma_{V}\right)^2=\left(\frac{19.6\times0.035}{48\times0.1507\times(10.2)^2}\times0.642\right)^2=3.4\times10^{-7}m.h^{-1}$$

Or

$$k_m=\sqrt{(3.4+2.82+3.4)\times10^{-7}+1.68\times10^{-10}+1.24\times10^{-8}}=9.87\times10^{-4}m.h^{-1}=2.74\times10^{-7}m.s^{-1}$$

Similarly, the uncertainty associated with the mass transfer coefficient for nickel (Run 10: at 12 V and 0.02357 $m^3.m^{-2}.s^{-1}$) was found to be $2.34\times10^{-7}\ m.s^{-1}$.

Appendix B: Summary of Experimental Runs

Appendix B1: Porous Aluminum Foam Cathode and Porous SS Anode

Table B1-1: Run 1

Conditions: @ **0.00471 $m^3.m^{-2}.s^{-1}$**; 10 V; T=25°C; pH = 5.6-6

Observations (#)	Time (h)	Ni^{++} Conc. ($mg.l^{-1}$)	Ni^{++} Removal (%)	Zn^{++} Conc. ($mg.l^{-1}$)	Zn^{++} Removal (%)
1	0	20.0	0.00	20.0	0.00
2	4	18.0	10.00	13.2	34.00
3	8	15.6	22.00	9.6	52.00
4	24	12.1	39.50	5.8	71.00
5	28	11.2	44.00	5.5	72.50
6	32	10.8	46.00	5.2	74.00
7	48	9.8	51.00	4.1	79.50

Table B1-2: Run 2

Conditions: @ **0.00943 $m^3.m^{-2}.s^{-1}$**; 10 V; T=25°C; pH = 5.6-6

Observations (#)	Time (h)	Ni^{++} Conc. ($mg.l^{-1}$)	Ni^{++} Removal (%)	Zn^{++} Conc. ($mg.l^{-1}$)	Zn^{++} Removal (%)
1	0	20.0	0.00	20.0	0.00
2	4	17.0	15.00	12.1	39.50
3	8	14.4	28.00	9.0	55.00
4	24	11.6	42.00	5.0	75.00
5	28	10.5	47.50	4.3	78.50
6	32	10.2	49.00	3.9	80.50
7	48	8.4	58.00	2.70	86.50

Table B1-3: Run 3

Conditions: @ **0.01414 $m^3.m^{-2}.s^{-1}$**; 10 V; T=25°C; pH = 5.6-6

Observations (#)	Time (h)	Ni^{++} Conc. ($mg.l^{-1}$)	Ni^{++} Removal (%)	Zn^{++} Conc. ($mg.l^{-1}$)	Zn^{++} Removal (%)
1	0	20.0	0.00	20.0	0.00
2	4	15.0	25.00	11.1	44.50
3	8	12.2	39.00	7.5	62.50
4	24	9.0	55.00	2.4	88.00
5	28	8.4	58.00	1.8	91.00
6	32	10.1	49.50	3.1	84.50
7	48	11.5	42.50	3.3	83.50

Appendix B2: Porous Corrugated Aluminum Cathode and Porous SS Anode

Table B2-1: Run 1

Conditions: @ **5 V**; 0.02357 $m^3.m^{-2}.s^{-1}$; T=25°C; pH = 5.6-6

Observations (#)	Time (h)	Ni^{++} Conc. ($mg.l^{-1}$)	Ni^{++} Removal (%)	Zn^{++} Conc. ($mg.l^{-1}$)	Zn^{++} Removal (%)
1	0	20	0.00	20.0	0.00
2	4	15.8	21.00	9.7	51.50
3	8	13.7	31.50	5.7	71.50
4	24	9	55.00	3.4	83.00
5	28	8.6	57.00	3.0	85.00
6	32	8.2	59.00	2.5	87.50
7	48	6.8	66.00	1.4	93.00

Table B2-2: Run 2

Conditions: @ **10 V**; 0.02357 $m^3.m^{-2}.s^{-1}$; T=25°C; pH = 5.6-6

Observations (#)	Time (h)	Ni^{++} Conc. ($mg.l^{-1}$)	Ni^{++} Removal (%)	Zn^{++} Conc. ($mg.l^{-1}$)	Zn^{++} Removal (%)
1	0	20.0	0.00	20.0	0.00
2	4	14.0	30.00	7.2	64.00
3	8	12.0	40.00	3.8	81.00
4	24	7.2	64.00	1.6	92.00
5	28	6.3	68.50	1.4	93.00
6	32	5.9	70.50	0.9	95.50
7	48	4.5	77.50	0.60	97.00

Table B2-3: Run 3

Conditions: @ **15 V**; 0.02357 $m^3.m^{-2}.s^{-1}$; T=25°C; pH = 5.6-6

Observations (#)	Time (h)	Ni^{++} Conc. ($mg.l^{-1}$)	Ni^{++} Removal (%)	Zn^{++} Conc. ($mg.l^{-1}$)	Zn^{++} Removal (%)
1	0	20.0	0.00	20.0	0.00
2	4	14.8	26.00	5.2	74.00
3	8	13.1	34.50	2.9	85.50
4	24	9.0	55.00	0.8	96.25
5	28	8.0	60.00	0.6	97.00
6	32	7.2	64.00	0.5	97.45
7	48	5.6	72.00	0.3	98.30

Table B2-4: Run 4

Conditions: @ **20 V**; 0.02357 $m^3.m^{-2}.s^{-1}$; T=25°C; pH = 5.6-6

Observations (#)	Time (h)	Ni^{++} Conc. ($mg.l^{-1}$)	Ni^{++} Removal (%)	Zn^{++} Conc. ($mg.l^{-1}$)	Zn^{++} Removal (%)
1	0	20.0	0.00	20	0.00
2	4	15.9	20.50	5	75.00
3	8	13.8	31.00	2.4	88.00
4	24	9.9	50.50	0.58	97.10
5	28	8.7	56.50	0.42	97.90
6	32	8.3	58.50	0.31	98.45
7	48	7.5	62.50	0.23	98.85

Table B2-5: Run 5

Conditions: @ **25 V**; 0.02357 $m^3.m^{-2}.s^{-1}$; T=25°C; pH = 5.6-6

Observations (#)	Time (h)	Ni^{++} Conc. ($mg.l^{-1}$)	Ni^{++} Removal (%)	Zn^{++} Conc. ($mg.l^{-1}$)	Zn^{++} Removal (%)
1	0	20.0	0.00	20.0	0.00
2	4	16.5	17.50	4.3	78.50
3	8	14.4	28.00	1.8	91.00
4	24	11	45.00	0.5	97.55
5	28	10.5	47.50	0.4	98.10
6	32	9.6	52.00	0.3	98.60
7	48	8.8	56.00	0.2	99.05

Table B2-6: Run 6

Conditions: @ **0.00471 $m^3.m^{-2}.s^{-1}$**; 10 V; T=25°C; pH = 5.6-6

Observations (#)	Time (h)	Ni^{++} Conc. ($mg.l^{-1}$)	Ni^{++} Removal (%)	Zn^{++} Conc. ($mg.l^{-1}$)	Zn^{++} Removal (%)
1	0	20	0.00	20.0	0.00
2	4	16.8	16.00	11.0	45.00
3	8	14.4	28.00	8.4	58.00
4	24	10.5	47.50	4.8	76.00
5	28	9.8	51.00	4.5	77.50
6	32	9.2	54.00	4.2	79.00
7	48	8	60.00	3.2	84.00

Table B2-7: Run 7

Conditions: @ **0.00943 $m^3.m^{-2}.s^{-1}$**; 10 V; T=25°C; pH = 5.6-6

Observations (#)	Time (h)	Ni^{++} Conc. ($mg.l^{-1}$)	Ni^{++} Removal (%)	Zn^{++} Conc. ($mg.l^{-1}$)	Zn^{++} Removal (%)
1	0	20.0	0.00	20	0.00
2	4	16.3	18.50	10.1	49.50
3	8	13.9	30.50	7.4	63.00
4	24	10.0	50.00	3.6	82.00
5	28	9.5	52.50	3.5	82.50
6	32	9.1	54.50	3.3	83.50
7	48	7.3	63.50	2.3	88.50

Table B2-8: Run 8

Conditions: @ **0.01414 $m^3.m^{-2}.s^{-1}$**; 10 V; T=25°C; pH = 5.6-6

Observations (#)	Time (h)	Ni^{++} Conc. ($mg.l^{-1}$)	Ni^{++} Removal (%)	Zn^{++} Conc. ($mg.l^{-1}$)	Zn^{++} Removal (%)
1	0	20.0	0.00	20.0	0.00
2	4	16.0	20.00	9.5	52.50
3	8	13.5	32.50	6.5	67.50
4	24	9.5	52.50	2.6	87.00
5	28	9.0	55.00	2.2	89.00
6	32	8.4	58.00	1.8	91.00
7	48	6.8	66.00	1.3	93.50

Table B2-9: Run 9

Conditions: @ **0.01886 $m^3.m^{-2}.s^{-1}$**; 10 V; T=25°C; pH = 5.6-6

Observations (#)	Time (h)	Ni^{++} Conc. ($mg.l^{-1}$)	Ni^{++} Removal (%)	Zn^{++} Conc. ($mg.l^{-1}$)	Zn^{++} Removal (%)
1	0	20	0.00	20	0.00
2	4	15	25.00	8.4	58.00
3	8	13.3	33.50	5.4	73.00
4	24	8.8	56.00	1.8	91.00
5	28	7.7	61.50	1.6	92.00
6	32	7.3	63.50	1.2	94.00
7	48	6	70.00	0.98	95.10

Table B2-10: Run 10

Conditions: @ **0.02357 $m^3.m^{-2}.s^{-1}$; 12 V;** T=25°C; pH = 5.6-6

Observations (#)	Time (h)	Ni^{++} Conc. ($mg.l^{-1}$)	Ni^{++} Removal (%)	Zn^{++} Conc. ($mg.l^{-1}$)	Zn^{++} Removal (%)
1	0	20.0	0.00	20.0	0.00
2	4	12.9	35.50	5.4	73.00
3	8	10.1	49.50	3.2	84.00
4	24	6.0	70.00	1.0	95.00
5	28	4.9	75.50	0.8	96.25
6	32	4.5	77.50	0.6	96.90
7	48	3.0	85.50	0.4	98.00